Technical Note: A hydrological routing scheme for the Ecosystem Demography model (ED2+R)

Fabio F. Pereira[1,*], Fabio Farinosi[1,2], Mauricio E. Arias[1, 3], Eunjee Lee[1,†], John Briscoe[1,#], and Paul R. Moorcroft[1]

[1]{Sustainability Science Program, Kennedy School of Government, Harvard University, Cambridge, MA 02138, USA}

[2]{Ca' Foscari University of Venice, Venice, Italy}

[3] Department of Civil and Environmental Engineering, University of South Florida, Tampa, FL 33620, USA

[*]{now at: Department of Renewable Energy Engineering, Federal University of Alagoas, Maceió, AL, Brazil }

[†] {now at: Goddard Earth Sciences Technology and Research, Universities Space Research Association, Columbia, MD, 21046. Current address: Global Modeling and Assimilation Office, NASA Goddard Space Flight Center, Greenbelt, MD 22071, USA}

[#] {Deceased - November 12th 2014}

Correspondence to: Fabio Farinosi (fabio.farinosi@gmail.com)

Abstract

Land surface models are excellent tools for studying how climate change and land use affect surface hydrology. However, in order to assess the impacts of earth processes on river flows, simulated changes in runoff need to be routed through the landscape. In this Technical Note, we describe the integration of the Ecosystem Demography (ED2) model with a hydrological routing scheme. The purpose of the study was to create a tool capable of incorporating the terrestrial ecosystem responses to climate, carbon dioxide, and land-use change –as simulated with terrestrial biosphere models– to hydrological predictions. The resulting ED2+R model calculates the lateral routing of surface and subsurface runoff resulting from the terrestrial

biosphere models' vertical water balance in order to determine spatio-temporal patterns of river flows within the simulated region. We evaluated the ED2+R model in the Tapajós, a 476,674 km^2 river basin in southeastern Amazonia, Brazil. The results showed that the integration of ED2 with the lateral routing scheme results in an adequate representation (Nash Sutcliff Efficiency up to 0.76, Kling Gupta Efficiency up to 0.86, Pearson's R up to 0.88, and Volume Ratio up to 1.06) of daily to decadal river flow dynamics in the Tapajós. These results are a consistent step forward with respect to the 'no river representation' common among terrestrial biosphere models as the native version of ED2.

1 Introduction

Understanding the impacts of deforestation (e.g., Lejeune et al. 2015; Medvigy et al. 2011; Andréassian 2004) and climate change (e.g., Jiménez-Cisneros et al. 2014) on the earth's water cycle has been a topic of substantial interest in recent years because of potential implications to ecosystems and society (e.g., Wohl et al. 2012; Brown et al., 2005). Analyses of impacts of climate change on the earth's water cycle are increasingly using terrestrial biosphere models, which are capable of estimating changes in the vertical water balance as a function of climate forcing and and/or land-use induced changes in canopy structure and composition (Zulkafli et al. 2013). Terrestrial biosphere models actively used for hydrological and earth systems sciences include: the Joint UK Land Environment Simulator (JULES) (Best et al. 2011; Clark et al. 2011); the Community Land Model (CLM) (Lawrence et al. 2011; Oleson et al. 2010); the Lund-Potsdam-Jena (LPJ) land model (Gerten et al. 2004; Sitch et al. 2003); the Max Plank Institute MPI-JSBACH model (Vamborg et al. 2011; Raddatz et al. 2007); and the Integrated Biosphere Simulator (IBIS) (Kucharik et al. 2000).

Initial formulations of the hydrological processes within terrestrial biosphere models were based on simple "bucket" model formulations (Cox et al. 1999 after Carson 1982). Moisture within each climatological grid cell of the domain was simulated in a single below-ground pool in which surface temperature and specific soil moisture factors determined evaporation, while runoff was equal to the bucket overflow (Cox et al. 1999; Carson 1982). Since that formulation, the hydrologic schemes within terrestrial biosphere models have become increasingly sophisticated. In the most recent generation of land surface models, water fluxes in and out of the soil column are vertically-resolved and take into account feedbacks among the different components, for instance, through an explicit formulation of the soil-plant-atmosphere

continuum that allows a detailed representation of the interactions between evapotranspiration, soil moisture and runoff (Clark et al. 2015).

To couple the calculation of the one-dimensional water balance to the estimation of daily river flows, there is the need to simulate multiple hydrological dynamics involved in the lateral flow propagation through the landscape, including the most complex hydraulic features of floodplains, lakes, and wetlands (Yamazaki et al. 2011). The first step towards representing the finer scale hydrodynamic processes responsible for patterns in river gauge observations, is to consider the topographic and geomorphological features that control water flow (Arora et al. 1999). The coarse spatial resolution of regional land surface models, due to computational constraints, does not allow to properly simulate complex hydrological dynamics determined by fine scale topography in river channels and floodplains (Yamazaki et al. 2011; Kauffeldt et al. 2016). However, the combination of the terrestrial models with routing schemes can be used to simulate the implications of global and regional environmental changes for flood/drought forecasting, water resources planning and management, and infrastructure development (Andersson et al. 2015). Consequently, several terrestrial biosphere models have been integrated with routing schemes. For example, JULES has been integrated with the Total Runoff Integrating Pathways (TRIP) to evaluate the accuracy of its estimates of annual streamflow (Oki et al. 1999). This integrated model was used after to investigate the status of the global water budget (Oki et al. 2001). Rost et al. (2008) also used a modelling framework composed of the global dynamic vegetation model, LPJ, and a simple water balance model to quantify the global consumption of water for rainfed and irrigated agriculture. An offline coupling of the dynamic vegetation model, ISIS, and HYDRA – which simulates the lateral transport of water through river, lakes and wetlands – was proposed in Coe et al. (2008) with the purpose of reproducing linkages between land use, hydrology and climate. Moreover, Liang et al. (1994) developed and tested the coupling of the well-known VIC model with a general circulation model (GCM) to improve the GCM's capability to capture the interactions between surface hydrology and atmosphere. For the same purpose, the MPI hydrological discharge model was validated with NCEP reanalysis and parametrized for simulating the river routing for climate analysis at global scale (Hagemann and Gates 2001; Hagemann and Dumenil 1997). Several routing schemes have been designed over time, including: normal depth, modified pulse, simple Muskingum, and Muskingum Cunge (USACE 1991). In particular, the semi-distributed kinematic wave routing Muskingum Cunge method has been recognized for its stability over different spatial and temporal modeling resolutions (USACE 1991; Miller and

Cunge 1975; Cunge 1969), and it was adopted in the most widely used regional scale hydrological models, such as VIC, SWAT, and MGB-IPH.

Recent studies have investigated regional patterns of rainfall and biosphere temperature as influenced by land- use (Ostberg et al. 2015; Bahn et al. 2014; Pearson et al. 2013). These studies have used historical reconstructions of land-use based on satellite information and data on agricultural production and population (Hurtt et al. 2006; Goldewijk 2001; Ramankutty and Foley 1999). These studies evidenced the occurrence of conversion of land from its natural state over the same time frame as observed fluctuations of rainfall and air temperature occurred, aspects fully analysed by terrestrial biosphere models. However, these modeling frameworks tend to assume global and regional changes in the biosphere as result of dynamics of vegetation in a collection of landscapes given by forests, deserts, and farmland only. Inland surface waters (e.g. rivers, lakes and wetlands) were not considered as an interactive component of the biosphere, and hence the climate system (Cole et al. 2007). A modeling framework that represents changes in inland surface waters (e.g. surface water area and volume) comes as one of the steps to understand the interactions between surface hydrology and climate.

The Ecosystem Demography (ED2) is a terrestrial biosphere model that simulates the coupled water, carbon, and energy dynamics of terrestrial land surfaces (Longo 2014; Medvigy et al. 2009; Moorcroft et al. 2001) to describe the coupled water, carbon and energy dynamics of heterogeneous landscapes (Hurtt et al. 2013; Medvigy et al. 2009; Moorcroft et al. 2001). ED2's ability to incorporate sub-grid scale ecosystem heterogeneity arising from land-use change makes the model suited for investigating how the combined impacts of changes in climate, atmospheric carbon dioxide concentrations, and land-cover affect terrestrial ecosystems. For example, ED2 was successfully used to simulate the carbon flux dynamics in the North American continent (Hurtt et al. 2002; Albani et al. 2006), and to assess the impacts on Amazonian ecosystems of changes in climate, atmospheric carbon dioxide and land use (Zhang et al. 2015). Moreover, ED2, coupled with a regional atmospheric circulation component, has been also successfully applied to assess the impacts of deforestation on the Amazonian climate (Knox et al. 2015; Swann et al. 2015). The mentioned studies were not aimed at assessing hydrological implications of changes in land use and climate. These works proved the validity of ED2 as a tool able to assess impacts from global and regional changes on ecosystem function, and built the basis for a possible development of an integrated tool aimed at analyzing hydrological implications. In this technical note, we describe the integration of ED2 with a

hydrological routing scheme. The hydrological routing scheme chosen was adapted from the MGB-IPH (Collischonn et al. 2007). This exercise is aimed at calculating the lateral propagation and attenuation of the surface and subsurface runoff resulting from the vertical balance calculations, reproducing in this way daily river flows through a large river basin. The advantage of the proposed model is the ability to predict the sensitivity of river flows to global and regional environmental changes as climate and land-use changes. The new product combines the advantages of biosphere and hydrological models, bringing together global, regional, and local scale hydrological dynamics in a single modeling framework. The resulting model is intended to be used as computational tool to explore the following research questions:

(1) How do current and future climate and land cover affect water availability in river systems?

(2) How can land-use driven changes influence the water availability for human activities (hydropower, food production, urban supply)?

(3) What are the implications of those changes for management of water and land resources?

These research questions are in line with key problems raised in the literature, focusing on the importance of large scale modelling and remote sensing to fill knowledge gaps in water resources and hydrological dynamics (Alsdorf et al. 2007; Prigent et al. 2007). The product obtained from this exercise was tested in the Tapajós basin, a large river system in southeastern Amazonia, Brazil.

2 Ecosystem Demography (ED2) model

ED2 is a terrestrial biosphere simulation model capable of representing biological and physical processes driving the dynamics of ecosystems as a function of climate and soil properties. Rather than using a conventional "ecosystem as big-leaf" assumption, ED2 is formulated at the scale of functional and age groups of plants. Ecosystem-scale dynamics and fluxes are calculated through a scaling procedure to reproduce macroscopic behavior of the ecosystem within each climatological grid-cell. It simulates ecosystem structure and dynamics as well as the corresponding carbon, energy, and water fluxes (Figure 1; Hurtt et al. 2013; Medvigy et al. 2009; Moorcroft et al. 2001). ED2 simulates the dynamics of different plant functional types subdivided into tiles with a homogeneous canopy (Swann et al. 2015; Medvigy et al. 2009).

The dynamic tiles represent the sub-grid scale heterogeneity in ecosystem composition within each cell. Grid cell size is determined by the resolution of meteorological forcing and soil characteristics data, typically from 1 to 0.001 degrees (~ 110 to 1 km). ED2 simulates biosphere dynamics taking into consideration natural disturbances, such as forest fires and plant mortality due to changing environmental conditions, as well as human-caused disturbances, such as deforestation and forest harvesting (Medvigy et al. 2009; Albani et al. 2006). Disturbances are expressed in the model as annual transitions between primary vegetation, secondary vegetation, and agriculture (cropland and pasture) (Albani et al. 2006). Natural disturbance, such as wildfire, is represented in the model by the transition from primary vegetation (forest in the case of the Amazon) to grassland-shrubland, and subsequently to secondary vegetation (forest re-growth); the abandonment of an agricultural area is represented with the conversion from grassland to secondary vegetation, while forest logging is represented by the transition from primary or secondary vegetation to grassland. The model is composed of several modules operating at multiple temporal and spatial scales, including plant mortality, plant growth, phenology, biodiversity, soil biogeochemistry, disturbance, and hydrology (Longo 2014; Medvigy et al. 2009). A selection of the main parameters and the input used for this study are presented in Table 1, and for a more complete description of the model, we refer the reader to the literature available (Zhang et al. 2015; Longo 2014; Kim et al. 2012; Medvigy et al. 2009; Moorcroft et al. 2001).

2.1 ED2 hydrology module

In this section, we describe in further detail the hydrological sub-component, most related to the topic of this specific study. The hydrological module of the ED2 model is derived from the Land Ecosystem-Atmospheric Feedback model (LEAF-2) (Walko et al. 2000). The model computes the water cycle through the vegetation, air-canopy space, and soils, which results in daily estimates of subsurface and surface runoff from each grid cell, isolated from the others in the domain. The number of soil layers and their thickness influence the accuracy with which the model is able to represent the gradients near the surface. Soil composition was derived from Quesada et al. (2010) and from the IGBP-DIS global soil data (Global Soil Data Task 2014). As described in Zhang et al. (2015), the mean fraction values of sand and clay were assigned to each grid-cell at 1 km resolution and then aggregated at 1 degree resolution. Due to limited data availability, soils were assumed to be homogeneous for a depth of 6 meters. Hydraulic

conductivity of the soil layers is a function of soil texture and moisture (Longo 2014). Groundwater exchange is a function of hydraulic conductivity, soil temperature and terrain topography. Water percolation is limited to the bottom layer by the subsurface drainage, determining the bottom boundary conditions. Vegetation historical records and land use transitions were derived from the Global Land Use Dataset (Hurtt et al. 2006). A more detailed description of the hydrological sub-component of the ED2 model is available in Longo (2014).

3 ED2 runoff routing scheme (ED2+R)

River routing schemes are commonly used to compute the lateral movement of water over land in hydrology models for large river basins. In this way, the prediction performance of models can be evaluated using river discharge measurements. The use of routing schemes was then extended to earth system models in order to capture the impacts of man-made structures (e.g. dams and reservoirs) and floodplain wetlands on the climate system (Li et al., 2011; Yamazaki et al., 2011).

Daily runoff estimates from ED2 were computed for specific grid cells independently; therefore a hydrological routing scheme was linked to this model in order to estimate flow attenuation and accumulation as water moves through the landscape. The hydrological routing scheme chosen was adapted from the original formulation of the MGB-IPH, a rainfall-runoff model that has been used extensively in large river basins in South America (Collischonn et al. 2007). This model was later developed using hydrodynamic solutions and floodplain coupling (Pontes et al. 2015; Paiva et al. 2013). Although the later development increased the modeling capabilities of the MGB-IPH in representing fine scale dynamics, given the regional application of our tool, for the ED2+R we decided to use the typical application of the MGB-IPH characterized by the Muskingum-Cunge approach. The original MGB-IPH model is composed of four different sub-models: soil water balance, evapotranspiration, intra-cell flow propagation, and inter-cell routing through the river network; only the catchment and river routing methods were utilized. The resulting ED2+R model computes the daily total volume of water passing through any given grid cell in the resulting drainage network in two separate steps: first, ED2 estimates of daily surface and subsurface runoff from each grid cell are divided into three linear reservoirs with different residence times to represent overland flow, interflow and groundwater flow (Figure 2). The reservoirs are used to determine the contribution and attenuation of river flow by different soil layers, characterized by different routing times. The sum of overland flow,

interflow, and groundwater flow is then moved from each grid cell into the drainage network, designed in the pre-processing phase using data from a digital elevation model (DEM) from the Shuttle Radar Topography Mission at a 90-meter resolution and the Cell Outlet Tracing with an Area Threshold algorithm (COTAT) (Reed 2003). Each DEM grid cell therefore becomes part of a flow path, which then accumulates water to a final downstream drainage network outlet. A complete description of the technique for defining drainage networks from DEMs employed in this study can be found in Paz et al. (2006). Once water reaches the drainage network, ED2+R adopts the Muskingum-Cunge numerical scheme for the solution of the kinematic wave equation, which also accounts for flow attenuation, using a finite-difference method as a function of river length, width, depth and roughness, as well as terrain elevation slope (Collischonn et al. 2007; Reed 2003). Statistical relationships for the river morphology were obtained as a function of the drainage area based on geomorphic data collected by Brazil's National Water Agency (ANA) and the Observation Service for the geodynamical, hydrological and biogeochemical control of erosion/alteration and material transport in the Amazon basin (HyBAM) at several gauging stations in the Amazon and Tocantins basins as presented by Coe et al. (2008). Further studies successfully derived geomorphological relations to estimate river geometric parameters and carry out hydrodynamic simulations of the Amazon River system using a similar approach (Paiva et al., 2013; Paiva et al., 2011). Multiple groups of grid cells with common hydrological features, or hydrological response units, can be created in order to parameterize and calibrate ED2+R. In our approach, hydrological traits associated with soil and land cover are primarily computed in ED2, thus we calibrated ED2+R at the subbasin level as delineated based on the DEM. Details about the calibration procedure are provided in the next section.

Model's performance was calculated through the adoption of widely used indicators:

- Pearson's R correlation coefficient (Pearson 1895), calculated as in Equation 1:

$$R = \frac{\sum sim*obs - \frac{(\sum sim)(\sum obs)}{n}}{\sqrt[2]{\left(\sum sim^2 - \frac{(\sum sim)^2}{n}\right)\left(\sum obs^2 - \frac{(\sum obs)^2}{n}\right)}} \quad (1)$$

Where sim and obs are the simulated and observed time series, while n is the number of time steps of the simulation period.

- Volume Ratio, calculated as ratio of the simulated (sim) and observed (obs) total water volume in the simulation period without consideration for the seasonal distribution of flow, as in Equation 2:

$$VR = Vol_{\text{sim}} / Vol_{\text{obs}} \qquad (2)$$

- Nash-Sutcliffe Efficiency (NSE) coefficient (Nash & Sutcliffe 1970), calculated as in Equation 3:

$$NSE = 1 - \frac{\sum_1^n |obs_i - sim_i|^2}{\sum_1^n |obs_i - \overline{obs_i}|^2} \qquad (3)$$

Where obs_i and sim_i are the observed and simulated data at time i, $\overline{obs_i}$ is the mean of the observed data, and n is number of time steps of the simulation period.

- Kling Gupta Efficiency (KGE) index, both 2009 and 2012 versions, calculated as in Equation 4:

$$KGE = 1 - \sqrt{\left(s[1](r-1)\right)^2 + \left(s[2](vr_{2009\ or\ 2012} - 1)\right)^2 + \left(s[3](\beta - 1)\right)^2} \quad (4)$$

Where, s are scaling factors; r is the Pearson's correlation coefficient; β is the ratio between the mean of the observed values and the mean of the simulated values; vr is the variability ratio, defined as vr_{2009} (simulated vs observed standard deviation ratio, Equation 5) for the 2009 method, and vr_{2012} (ratio of coefficient of variation of simulated and coefficient of variation of observed values, Equation 6) for the 2012 method (Kling et al. 2012; Gupta et al. 2009).

$$vr_{2009} = \sigma_{sim} / \sigma_{obs} \qquad (5)$$

$$vr_{2012} = \frac{CV_{sim}}{CV_{obs}} = \frac{\sigma_{sim} / \mu_{sim}}{\sigma_{obs} / \mu_{obs}} \qquad (6)$$

The optimal value for the Pearson's R, VR, NSE, and KGE indexes is 1: the closer to this value, the more accurately the model reproduces the observed values.

Missing observations in the river flow records (HYBAM and ANA) were filled via linear spatial and temporal interpolation between the series in neighboring gauge stations (Equation 7):

$$Obs_y(t) = K + \beta_1 \cdot Obs_z(t) + \beta_2 \cdot Obs_q(t) + \beta_3 \cdot Obs_y(t - 365) + \beta_4 \cdot Obs_y(t + 365) \qquad (7)$$

Where *z*, *y*, and *q* are three gauge stations with time series highly correlated (Pearson's $r \geq 0.85$), and *t* expresses time in days. The estimated β coefficients in Equation 7 were used for the estimation of the missing observations in the site *y* (Table 2). The interpolation of the gauge historical records was necessary to have continuous time series with a sufficient number of observations to calibrate and validate the ED2+R application in the basin.

For the presentation of the results, in order to compare the simulated and observed values, we also used flow duration curves (FDCs). FDCs are a cumulate frequency plots that show the percentage of simulations steps (days in the case presented in this study) in which the discharge is likely to equal or exceed a specific value, without taking into consideration the sequence of the occurrence.

4 Case Study: Tapajós river basin

We parameterized and evaluated the ED2+R formulation for the Tapajós River Basin, the fifth largest tributary of the Amazon. It drains an area of 476,674 km^2 in southeastern Amazonia, within the Brazilian states of Mato Grosso, Pará and Amazonas. The main rivers in the basin are the Tapajós (with a length greater than 1,800 km and average discharge of 11,800 $m^3 s^{-1}$), Juruena (length of approximately 1,000 km and discharge of 4,700 $m^3 s^{-1}$) , and Teles Pires (also known with the name Sao Manoel, about 1,600 km long and average discharge of 3,700 $m^3 s^{-1}$). The river system flows northwards, with terrain elevation ranging from about 800 meters above sea level in the southern part, to a few meters above sea level in its confluence with the Amazon river (ANA, 2011). The basin ecosystems are mainly represented by tropical evergreen rainforests in the northern part (in the states of Amazonas and Pará), and Cerrado dry vegetation in the south (Mato Grosso). Precipitation range from about 1,500 mm y^{-1} in the headwaters (southern part), to about 2,900 mm y^{-1} towards the basin's outlet (Figure 3 a - b). Rainfall temporal distribution is characterized by a clear seasonal distinction; total precipitation in the wet season (September to May) could be as high as 400 mm $month^{-1}$ in the most tropical areas, whereas in the dry season (June to August), precipitation is close to zero in the Cerrado and as low as 50 mm $month^{-1}$ in the wetter areas (Mohor et al., 2015). As a result of the large rainfall seasonal variability, river flows are also extremely variable: the mean monthly flow of the Tapajós river range between about 2,300 and 28,600 $m^3 s^{-1}$ according to the historical records used for the calibration of our model. Soils vary from those typically seen in the

Brazilian shield in the south of the basin to alluvial sediments in the north. Land-use, almost completely represented by primary forest until the 1970s, was radically changed in recent decades. As estimated from the land-use/land-cover dataset set used in this study (Hurtt et al. 2006), in the late 2000s only about 56% of the basin (270,000 km^2) was covered by the original vegetation cover. Large parts of the basin laying in the territory of Mato Grosso, were cleared to make room for agricultural and livestock production, while vast areas around the border between the state of Pará and Mato Grosso were cleared for cattle production. The northern portion of the basin is largely protected by natural parks or indigenous lands, but large deforestation hotspots could be identified around the cities of Santarem and Itaituba and along the main transportation routes (Figure 3c). For a more detailed description of the basin's physical characteristics and historical analysis of trends in deforestation, precipitation and discharge, we refer the reader to Arias et al. and Farinosi et al. (under review).

For calibration purposes the basin was divided into seven sub-basins, each of them with a corresponding gauge for which historical daily river flow observations were available (Figure 4a). The domain was gridded with a spatial resolution of 0.5° by 0.5°, roughly corresponding to 55 km by 55 km. Simulations were carried out for the period 1970-2008. The ED2 model was forced using reconstructed climate (Sheffield et al. 2006) and land use/land cover data (Hurtt et al. 2006; Soares-Filho et al. 2006) at 1-degree spatial resolution. The original meteorological dataset has a 3-hour temporal resolution, which was downscaled to an hourly resolution, as described in Zhang et al. (2015). In this technical note, we describe the calibration of the flow routing component of the ED2+R. The parameterization of the ED2 terrestrial biosphere model was developed and evaluated independently using eddy-flux tower observations of carbon, water, and energy fluxes and forest inventory observations of above-ground biomass dynamics. Further details are available elsewhere (Zhang et al. 2015, Longo 2014).

ED2+R Model Calibration: The ED2+R model was manually calibrated using gauge observations (HYBAM and ANA) spanning a period of 17 years, from 1976 to 1992 (the period 1970-1975 was not considered in order to avoid simulation initiation effects) through a two-step procedure, as highlighted in Figure 2. The first step is the partitioning of the flows from the two reservoirs (surface and sub-surface) of the ED2 biosphere model to the three reservoirs (surface, intermediate, base) of the ED2+R routed biosphere model (parameters α and β in Figure 2). In particular, α (ranging from 0 to 1, or from 0% to 100%) represents the share of ED2 surface runoff allocated to the ED2+R surface reservoir. The remaining part $(1 - \alpha)$ is

allocated to the ED2+R intermediate reservoir. β represents a similar partitioning coefficient for the ED2 sub-surface reservoir to the ED2+R intermediate and base reservoirs. The second step relates to the adjustment of the residence times of the water flows in the three reservoirs for each of the grid cells in each of the subbasins (overland, intermediate, and groundwater flows – *CS*, *CI*, *CB* in Figure 2).

In the first step, following the methodology described by Anderson (2002), the sensitivity of the α and β parameters was tested by running the model multiple times (>30). For each run, the Nash-Sutcliffe indicator (NSE) (Nash & Sutcliffe 1970) was quantified comparing the results of the simulation to historical flow observations. The combinations of the α and β parameters characterized by the largest NSE were selected. Parameters α and β were assumed to be uniform for the whole basin. Figure 5 shows the different combinations of the α and β parameters introduced in Figure 2. The color bar indicates the NSE resulting from the comparison between the simulated and observed river flow values obtained using different combinations of the parameters α (x axis) and β (y axis). The chosen combination (indicated by an x in Figure 5) lies in one of the optimal combination areas (NSE ~ 0.8).

In the second step, the residence times (τ) of flow within the ED2+R reservoirs of each grid cell in the domain were calibrated (*CS*, *CI*, and *CB* in Figure 2). The calibration procedure characterizing the second step is similar to the previous one but in this case the calibration is repeated for each subbasin sequentially; the calibration process was conducted from the furthest upstream subbasins – headwaters – to the final outlet of the basin (Anderson 2002). The model was run multiple times (between 30 and 50 per subbasin) with different combinations of the three parameters (*CS*, *CI*, and *CB* in Figure 2); for each run, the goodness-of-fit was quantified. This allowed us to design a sensitivity curve of the model to different combinations of the three parameters for each of the seven subbasins, and to select the combination that best approaches the historical observations. Figure 6 shows how the model is sensitive to marginal variation in initial conditions of baseflow, particularly in the upstream section (i.e. UTP - Upper Teles Pires, UJ – Upper Juruena, and LTP – Lower Teles Pires). Changes in initial groundwater were controlled by the initialization five year period, thus contributions to the downstream part of the basin had minimal impact (i.e. UT and LT - Upper and Lower Tapajós).

Figure 7 describes the calibration of the residence time for each of the subbasins. The different combinations of the values assigned to the parameters *CS*, *CI*, and *CB* significantly affect the overall goodness-of-fit of the river flow simulations (NSE indicator). The calibration process

was conducted from the furthest upstream subbasins – headwaters – (UTP – Upper Teles Pires, UJ – Upper Juruena, and JA – Jamanxim) to the final outlet of the basin (LT – Lower Tapajós). The different combinations are marked with the corresponding NSE value; the optimal combination is marked in red (Figure 7).

The period 1993-2008 was used for model evaluation. Comparison between observations and simulated flows (goodness-of-fit) were carried out using Pearson's R correlation coefficient (Pearson 1895), volume ratio (VR), the Nash-Sutcliffe Efficiency (NSE) coefficient (Nash & Sutcliffe 1970), and the Kling Gupta Efficiency (KGE) index (Kling et al. 2012; Gupta et al. 2009) (Table 3).

5 Results

The integration of the routing scheme with ED2 increases the ability of the model to reproduce the observed temporal variations in river flows at the basin outlet (Figure 8). This statement applies to all of the sub-basins, as the application of the routing scheme improved the model's performance between simulated and observed values with respect to all the four measures selected (Nash-Sutcliffe (NSE), Kling Gupta (KGE), Pearson's R correlation , and volume ratio) (Table 3). Both routed (ED2+R) and non-routed (ED2) simulation results manage to reproduce the observed water availability (quantity of water available) in the basin in terms of volume. The volume ratio at the furthest downstream sub-basin (Lower Tapajós), in fact, ranges around the optimal value for both validation and calibration periods (ED2 1.11-1.13, ED2+R 1.06-1.13). The routing scheme improves the ability of the model to reproduce the spatio-temporal distribution of water flows across the basin: both the NSE and the KGE indexes reached values ranging between 0.76 and 0.86 in the calibration, and 0.68-0.80 in the validation period (Table 3). Also, the correlation values confirm the results of the other indexes, reaching 0.88 for the calibration and 0.86 for the validation period. The performance of the presented tool is evident also analyzing FDCs (Figure 9 a - g). The adoption of the river routing scheme allows a more realistic representations of the high discharge values (flow equaled or exceeded 0 to 20/30% of the time), and low discharge values (flow equaled or exceeded 60 to 100% of the time) in all the sections of the basin (Figure 9). The model's performance in simulating river flows is generally more robust in the downstream sub-basins (NSE 0.68-0.77, and KGE 0.76-0.84 in the Upper and Lower Tapajós) and poorer in the headwaters (NSE 0.28-0.45, and KGE 0.38-0.61 in the Upper Juruena and Upper Teles Pires). In the Upper Teles Pires and Upper

Juruena, the model achieved the lowest NSE (0.28 and 0.29 respectively in the calibration, and 0.37 and 0.45 in the validation period), and KGE values (0.61 and 0.50 calibration, and 0.63 and 0.38 validation). Although water volumes are correctly reproduced in both the sub-basins (VR between 1.01 and 0.98 in the calibration, and 1.03 and 1.01 in the validation period), the seasonal variability is less accurate (correlation 0.64-0.68, and 0.63-0.54). The KGE, NSE and correlation indices are closer to the optimal value in the central and lower part of the basin, in particular in the Lower Juruena (calibration - NSE 0.65, KGE 0.64, correlation 0.82; validation - NSE 0.63, KGE 0.67, correlation 0.81), Lower Teles Pires (calibration - NSE 0.71, KGE 0.67, correlation 0.85; validation - NSE 0.67, KGE 0.60, correlation 0.85), Upper Tapajós (calibration - NSE 0.77, KGE 0.82, correlation 0.88; validation - NSE 0.75, KGE 0.81, correlation 0.88), and Lower Tapajós (calibration - NSE 0.76, KGE 0.83, correlation 0.88; validation - NSE 0.68, KGE 0.76, correlation 0.82) (Table 3).

FDCs, representing the probability of the flow values to exceed a specific discharge, highlight the positive effect of the application of the routing scheme in ED2+R across the entire range of flow variability (Figure 9). The simulated FDCs follow the same shape of the observed ones in the furthest upstream subbasins, especially in the cases of the Upper Juruena and Upper Teles Pires, implying that the routing scheme is effective in maintaining the simulated discharge range (Upper Juruena 1,200-2,480 m^3 sec^{-1}, Upper Teles Pires 393-4,130 m^3 sec^{-1}) in line with the observations (1,030-2,400 and 302–2,767 m^3 sec^{-1}, respectively). This is especially true for the lowest flows, where the error between simulated and observed curves is lower than 15% (Figure 9 a-b, Figure A.1). Regarding the intermediate subbasins, Lower Juruena and Lower Teles Pires, flood duration curves show that the model overestimates the lowest values of the distribution up by approximately 30% of the observed values (flow equaled or exceeded 60 to 100% of the time in Figure 9 c–d). Similar overestimation of the model could be noticed in the furthest downstream subbasins, Upper and Lower Tapajós (Figure 9 e–g). The overestimation of the lower discharge values highlighted in Figure 9g, is also evident in the multiyear hydrograph (Figure 8), which shows that the ED2+R simulation results overestimate (by about 40% on average in the discharge values included in the range 60 to 100% in Figure 9 g) the observations during the dry seasons of the period under consideration.

6 Discussion

As the results in Table 3 and Figures 8 - 9 show, the one-way integration of ED2 with a routing scheme increases the performance of simulated daily discharges. Although this could appear obvious from a hydrological modeling perspective, the significance of this study lies in the fact that terrestrial biosphere models, which are widely applied to examine the impacts of climate and land use on the hydrology of the land surface, are typically "no river representation" models. The incorporation of ecosystem responses to climate, carbon dioxide, and land-use changes simulated by terrestrial biosphere models with hydrological modeling improves the representation of the hydrological characteristics of basins characterized by large forest cover and/or large deforestation rates. In applications in the tropics, the one-way integration of the terrestrial biosphere model and the routing scheme (i.e. the two tools are not fully coupled) could lead to a partially inaccurate representation of the seasonally flooded ecosystems, a relevant aspect as documented in the literature (Cole et al. 2007).

As seen in Figure 9, the performance of the model in simulating river flows in the basin is generally higher in the downstream sub-basins and poorer in the headwaters. Several factors are likely to cause this issue, both from the simulation of the hydrological dynamics in ED2, the flow partitioning (α and β parameters), and the basin hydraulic characteristics in ED2+R. The accurate calibration of the biosphere model with flux tower observations (Zhang et al. 2015; Longo et al. 2014) and the optimization of the flow partitioning, make us believe that this is due to the relatively coarse spatial resolution of the model in combination with the limitations typical of most land surface models in capturing the interactions with deep groundwater (Lobligeois et al. 2014; Zulkafli et al. 2013; Smith et al. 2004). We believe that the error is arising from the complexities associated with deep soils present in the headwaters of the Tapajós basin. In particular, in the model application developed, soil layers are represented to a depth of 6 meters (Table 1), which might be too shallow to more realistically represent the conditions in the headwaters of the basin. The importance of groundwater is also evident from the calibration of the residence time of the groundwater flow: as shown in Figure 7, in fact, especially in the headwaters, even small variations in the CB parameter largely affect the model performance (specifically quantified with NSE in Figure 7). The combined effect of groundwater interactions and spatial resolution is more evident in the upstream subbasins because of the greater marginal contribution of baseflow in these areas. Surface flow accumulation, in fact, is lower in the headwaters. Therefore, in relative terms, the role of

baseflow is more relevant in this portion of any basin. Further downstream, the effect of groundwater interactions and spatial resolution is, at least in part, masked by the larger rainfall-runoff contribution and the overall flow accumulation from the upstream subbasins. Other recent hydrological simulations of the Tapajós have obtained higher accuracy (e.g. Mohor et al. 2015; Collischonn et al. 2008; Coe et al. 2008); however, these simulations were set up discretizing the basin into a finer spatial resolution grid (9 to 20 km versus ~ 55 km grid cells) and using hydrological tools able to reproduce highly detailed hydrodynamic characteristics of complex river systems (i.e. floodplain, lakes, wetlands, backwater effects) that are out of the scope of the tool presented in this study. The advantage of the ED2+R model is the ability to study the sensitivity of the river flows to global and regional changes as computed by traditional terrestrial biosphere models, but adding a more detailed hydrological feature with respect to a very simplistic- of no-river representation. The coarse spatial resolution of the global datasets used as input for ED2+R is, however, a limiting factor. Higher resolution climatological data, vegetation, and land use datasets, while allowing a finer resolution of the hydrological grid, are expected to improve the performance of the model providing more detailed hydrological processes. In general, the tool can be used to study how different hydrological systems are being affected by changes in climate forcing and changes in ecosystem composition and structure arising from the combination of: changing climate, rising atmospheric carbon dioxide, and land-use transformation. Additionally, ED2+R could potentially bridge one of the missing gaps for diagnosing and assessing feedbacks between atmosphere and biosphere with inland surface waters being represented as a dynamic system.

7 Conclusion

In this Technical Note, we present the integration of the terrestrial biosphere model Ecosystem Demography 2 (ED2) with the Muskingum-Cunge routing scheme. We tested the integrated model (ED2+R) in the Tapajós river basin, a large tributary of the Amazon in Brazil, for the period 1970-2008. The results showed that the integration of a biosphere model with a routing scheme improves the ability of the land surface simulation to reproduce the hydrological and river flow dynamics at the basin scale. The main limitations highlighted in this case study were linked to the relatively coarse spatial resolution of the model and the rough representation of groundwater flow typical of this kind of models. Moreover, the terrestrial biosphere model ED2 and the routing scheme are presented here in a one-way integration. The full coupling of the

routing scheme and ED2 could further improve the ability to reproduce the water balance considering flooded ecosystems, a relevant feature in the simulation of environments like the tropical forest, where local evapotranspiration plays a primary role in the specific ecosystem's dynamics. In this first integration, our goal was to give the possibility to the terrestrial biosphere model to reproduce river flows through a routing scheme. With a fully coupled (i.e. two-way) integration, the model would be able to determine the grid cells that are likely to be saturated and use this information for the modeling of the ecosystem's dynamics. For instance, this could determine the increase of the mortality rate of plants that are sensitive to inundation. An additional limitation of the model, could be identified in its inability to reproduce highly detailed hydrological dynamics of complex river systems (as for instance, floodplain hydraulic features, or backwater effects), however, such a detailed hydrological complexity was out of the scope of this study. Future efforts will be oriented towards the resolution of the highlighted limitations and current research is focusing on the application of ED2+R on understanding historical changes and future projections of the impacts of climate change and deforestation on the Amazon's water resources.

Author's contribution

F. Pereira, P. Moorcroft and J. Briscoe designed the study; F. Pereira developed the ED2+R model code; F. Farinosi, M. Arias, and E. Lee calibrated the model and carried out the analysis; F. Farinosi, M. Arias and P. Moorcroft wrote the paper.

Acknowledgements

This work was conducted while F. F. Pereira, F. Farinosi, E. Lee, and M. E. Arias were Giorgio Ruffolo Fellows in the Sustainability Science Program at Harvard University. F. Farinosi was also funded through a doctoral scholarship by Ca' Foscari University of Venice. Support from Italy's Ministry for Environment, Land and Sea is gratefully acknowledged. We would like to thank Marcos Longo for letting us use one of his figures, and Angela Livino for the useful comments. The authors would like to dedicate this study to the late Professor John Briscoe (1948 - 2014), who envisioned and co-led the Amazon Initiative of Harvard's Sustainability Science Program. We are grateful to the Editor, Professor Graham Jewitt, and to the two Anonymous Referees for the valuable comments received during the review process.

References

Albani, M., Medvigy, D., Hurtt, G. C. and Moorcroft, P. R.: The contributions of land-use change, CO 2 fertilization, and climate variability to the Eastern US carbon sink, Glob. Chang. Biol., 12(12), 2370–2390, doi:10.1111/j.1365-2486.2006.01254.x, 2006.

Alsdorf, D. E., Rodríguez, E. and Lettenmaier, D. P.: Measuring surface water from space, Rev. Geophys., 45(2), RG2002, doi:10.1029/2006RG000197, 2007.

ANA: Plano Estratégico de Recursos Hídricos da Bacia Amazônica – Afluentes da Margem Direita (in Portuguese), Brasilia, Brazil, Brazil. [online] Available from: http://margemdireita.ana.gov.br/, 2011.

Anderson, E. A.: Calibration of Conceptual Models for Use in River Forecasting. [online] Available from: http://www.nws.noaa.gov/oh/hrl/calb/calibration1102/main.htm, 2002.

Andersson, J. C. M., Pechlivanidis, I. G., Gustafsson, D., Donnelly, C. and Arheimer, B.: Key factors for improving large-scale hydrological model performance, Eur. Water, (49), 77–88, 2015.

Andréassian, V.: Waters and forests: from historical controversy to scientific debate, J. Hydrol., 291(1-2), 1–27, doi:10.1016/j.jhydrol.2003.12.015, 2004.

Arias, M. E., Lee, E., Farinosi, F., Pereira, F. F., Moorcroft, P. R. and Briscoe, J.: Decoupling the effects of deforestation and climate variability in large tropical river basins (under review), J. Hydrol., n.d.

Arora, V. K., Chiew, F. H. S. and Grayson, R. B.: A river flow routing scheme for general circulation models, J. Geophys. Res., 104(D12), 14347, doi:10.1029/1999JD900200, 1999.

Bahn, M., Reichstein, M., Dukes, J. S., Smith, M. D. and McDowell, N. G.: Climate-biosphere interactions in a more extreme world, New Phytol., 202(2), 356–359, doi:10.1111/nph.12662, 2014.

Baker, T. R., Phillips, O. L., Malhi, Y., Almeida, S., Arroyo, L., Di Fiore, A., Erwin, T., Killeen, T. J., Laurance, S. G., Laurance, W. F., Lewis, S. L., Lloyd, J., Monteagudo, A., Neill, D. A., Patino, S., Pitman, N. C. A., M. Silva, J. N. and Vasquez Martinez, R.: Variation in wood density determines spatial patterns in Amazonian forest biomass, Glob. Chang. Biol., 10(5), 545–562, doi:10.1111/j.1365-2486.2004.00751.x, 2004.

Best, M. J., Pryor, M., Clark, D. B., Rooney, G. G., Essery, R. . L. H., Ménard, C. B., Edwards, J. M., Hendry, M. A., Porson, A., Gedney, N., Mercado, L. M., Sitch, S., Blyth, E., Boucher, O., Cox, P. M., Grimmond, C. S. B. and Harding, R. J.: The Joint UK Land Environment Simulator (JULES), model description – Part 1: Energy and water fluxes, Geosci. Model Dev., 4(3), 677–699, doi:10.5194/gmd-4-677-2011, 2011.

Brown, A. E., Zhang, L., McMahon, T. A., Western, A. W. and Vertessy, R. A.: A review of paired catchment studies for determining changes in water yield resulting from alterations in vegetation, J. Hydrol., 310(1-4), 28–61, doi:10.1016/j.jhydrol.2004.12.010, 2005.

Calvo-Alvarado, J., McDowell, N. and Waring, R.: Allometric relationships predicting foliar biomass and leaf area:sapwood area ratio from tree height in five Costa Rican rain forest species, Tree Physiol., 11, 1601–1608, 2008.

Carson, D.: Current parametrisations of land-surface processes in atmospheric general circulation models, in Land surface processes in atmospheric general circulation models, edited by P. Eagleson, Cambridge University Press, Cambridge, UK., 1982.

Clark, D. B., Mercado, L. M., Sitch, S., Jones, C. D., Gedney, N., Best, M. J., Pryor, M., Rooney, G. G., Essery, R. L. H., Blyth, E., Boucher, O., Harding, R. J., Huntingford, C. and Cox, P. M.: The Joint UK Land Environment Simulator (JULES), model description – Part 2: Carbon fluxes and vegetation dynamics, Geosci. Model Dev., 4(3), 701–722, doi:10.5194/gmd-4-701-2011, 2011.

Clark, M. P., Fan, Y., Lawrence, D. M., Adam, J. C., Bolster, D., Gochis, D. J., Hooper, R. P., Kumar, M., Leung, L. R., Mackay, D. S., Maxwell, R. M., Shen, C., Swenson, S. C. and Zeng, X.: Improving the representation of hydrologic processes in Earth System Models, Water Resour. Res., 51(8), 5929–5956, doi:10.1002/2015WR017096, 2015.

Coe, M. T., Costa, M. H. and Howard, E. A.: Simulating the surface waters of the Amazon River basin: impacts of new river geomorphic and flow parameterizations, Hydrol. Process., 22(14), 2542–2553, doi:10.1002/hyp.6850, 2008.

Cole, J. J., Prairie, Y. T., Caraco, N. F., McDowell, W. H., Tranvik, L. J., Striegl, R. G., Duarte, C. M., Kortelainen, P., Downing, J. A., Middelburg, J. J. and Melack, J.: Plumbing the Global Carbon Cycle: Integrating Inland Waters into the Terrestrial Carbon Budget, Ecosystems, 10(1), 172–185, doi:10.1007/s10021-006-9013-8, 2007.

Cole, T. G. and Ewel, J. J.: Allometric equations for four valuable tropical tree species, For. Ecol. Manage., 229(1-3), 351–360, doi:10.1016/j.foreco.2006.04.017, 2006.

Collischonn, B., Collischonn, W. and Tucci, C. E. M.: Daily hydrological modeling in the Amazon basin using TRMM rainfall estimates, J. Hydrol., 360(1-4), 207–216, doi:10.1016/j.jhydrol.2008.07.032, 2008.

Collischonn, W., Allasia, D., Da Silva, B. C. and Tucci, C. E. M.: The MGB-IPH model for large-scale rainfall—runoff modelling, Hydrol. Sci. J., 52(5), 878–895, doi:10.1623/hysj.52.5.878, 2007.

Cox, P. M., Betts, R. A., Bunton, C. B., Essery, R. L. H., Rowntree, P. R. and Smith, J.: The impact of new land surface physics on the GCM simulation of climate and climate sensitivity, Clim. Dyn., 15(3), 183–203, doi:10.1007/s003820050276, 1999.

Cunge, J. A.: On The Subject Of A Flood Propagation Computation Method (Musklngum Method), J. Hydraul. Res., 7(2), 205–230, doi:10.1080/00221686909500264, 1969.

Farinosi, F., Arias, M. E., Lee, E., Longo, M., Pereira, F. F., Livino, A., Moorcroft, P. R. and Briscoe, J.: Future climate and land use change impacts on river flows in the Tapajós Basin in the Brazilian Amazon (under review), Earth's Futur., n.d.

Gerten, D., Schaphoff, S., Haberlandt, U., Lucht, W. and Sitch, S.: Terrestrial vegetation and water balance—hydrological evaluation of a dynamic global vegetation model, J. Hydrol., 286(1-4), 249–270, doi:10.1016/j.jhydrol.2003.09.029, 2004.

Global Soil Data Task: Global Soil Data Products CD-ROM Contents (IGBP-DIS). Data Set, Oak Ridge, Tennessee, U.S.A., 2014.

Goldewijk, K. K.: Estimating global land use change over the past 300 years: The HYDE Database, Global Biogeochem. Cycles, 15(2), 417–433, doi:10.1029/1999GB001232, 2001.

Gupta, H. V., Kling, H., Yilmaz, K. K. and Martinez, G. F.: Decomposition of the mean squared error and NSE performance criteria: Implications for improving hydrological modelling, J. Hydrol., 377(1-2), 80–91, doi:10.1016/j.jhydrol.2009.08.003, 2009.

Hagemann, S. and Dumenil, L.: A parametrization of the lateral waterflow for the global scale, Clim. Dyn., 14(1), 17–31, doi:10.1007/s003820050205, 1997.

Hagemann, S. and Gates, L. D.: Validation of the hydrological cycle of ECMWF and NCEP reanalyses using the MPI hydrological discharge model, J. Geophys. Res., 106(D2), 1503, doi:10.1029/2000JD900568, 2001.

Hurtt, G. C., Pacala, S. W., Moorcroft, P. R., Caspersen, J., Shevliakova, E., Houghton, R. A. and Moore, B.: Projecting the future of the U.S. carbon sink, Proc. Natl. Acad. Sci., 99(3), 1389–1394, doi:10.1073/pnas.012249999, 2002.

Hurtt, G. C., Frolking, S., Fearon, M. G., Moore, B., Shevliakova, E., MALYSHEV, S., PACALA, S. W. and Houghton, R. A.: The underpinnings of land-use history: three centuries of global gridded land-use transitions, wood-harvest activity, and resulting secondary lands, Glob. Chang. Biol., 12(7), 1208–1229, doi:10.1111/j.1365-2486.2006.01150.x, 2006.

Hurtt, G. C., Moorcroft, P. R. and Pacala, S. W.: Ecosystem Demography Model: Scaling Vegetation Dynamics Across South America, Ecosyst. Demogr. Model Scaling Veg. Dyn. Across South Am. Model Prod. [online] Available from: http://daac.ornl.gov/MODELS/guides/EDM_SA_Vegetation.html, 2013.

Jiménez-Cisneros, B. E., Oki, T., Arnell, N. W., Benito, G., Cogley, J. G., Döll, P., Jiang, T. and Mwakalila, S. S.: Freshwater resources., in Climate Change 2014: Impacts, Adaptation, and Vulnerability. Part A: Global and Sectoral Aspects. Contribution of Working Group II to the Fifth Assessment Report of the Intergovernmental Panel on Climate Change, edited by C. B. Field, V. R. Barros, D. J. Dokken, K. J. Mach, M. D. Mastrandrea, T. E. Bilir, M. Chatterjee, K. L. Ebi, Y. O. Estrada, R. C. Genova, B. Girma, E. S. Kissel, A. N. Levy, S. MacCracken, P. R. Mastrandrea, and L. L. White, pp. 229–269., Cambridge University Press, ambridge, United Kingdom and New York, NY, USA. [online] Available from: https://ipcc-wg2.gov/AR5/images/uploads/WGIIAR5-Chap3_FINAL.pdf, 2014.

Kauffeldt, A., Wetterhall, F., Pappenberger, F., Salamon, P. and Thielen, J.: Technical review of large-scale hydrological models for implementation in operational flood forecasting schemes on continental level, Environ. Model. Softw., 75, 68–76, doi:10.1016/j.envsoft.2015.09.009, 2016.

Kim, Y., Knox, R. G., Longo, M., Medvigy, D., Hutyra, L. R., Pyle, E. H., Wofsy, S. C., Bras, R. L. and Moorcroft, P. R.: Seasonal carbon dynamics and water fluxes in an Amazon rainforest, Glob. Chang. Biol., 18(4), 1322–1334, doi:10.1111/j.1365-2486.2011.02629.x, 2012.

Kling, H., Fuchs, M. and Paulin, M.: Runoff conditions in the upper Danube basin under an ensemble of climate change scenarios, J. Hydrol., 424-425, 264–277, doi:10.1016/j.jhydrol.2012.01.011, 2012.

Knox, R. G., Longo, M., Swann, A. L. S., Zhang, K., Levine, N. M., Moorcroft, P. R. and Bras, R. L.: Hydrometeorological effects of historical land-conversion in an ecosystem-atmosphere model of Northern South America, Hydrol. Earth Syst. Sci., 19(1), 241–273, doi:10.5194/hess-19-241-2015, 2015.

Kucharik, C. J., Foley, J. A., Delire, C., Fisher, V. A., Coe, M. T., Lenters, J. D., Young-Molling, C., Ramankutty, N., Norman, J. M. and Gower, S. T.: Testing the performance of a dynamic global ecosystem model: Water balance, carbon balance, and vegetation structure, Global Biogeochem. Cycles, 14(3), 795–825, doi:10.1029/1999GB001138, 2000.

Lawrence, D. M., Oleson, K. W., Flanner, M. G., Thornton, P. E., Swenson, S. C., Lawrence, P. J., Zeng, X., Yang, Z.-L., Levis, S., Sakaguchi, K., Bonan, G. B. and Slater, A. G.: Parameterization improvements and functional and structural advances in Version 4 of the Community Land Model, J. Adv. Model. Earth Syst., 3(3), M03001, doi:10.1029/2011MS000045, 2011.

Lejeune, Q., Davin, E. L., Guillod, B. P. and Seneviratne, S. I.: Influence of Amazonian deforestation on the future evolution of regional surface fluxes, circulation, surface temperature and precipitation, Clim. Dyn., 44(9-10), 2769–2786, doi:10.1007/s00382-014-2203-8, 2015.

Li, R., Chen, Q. and Ye, F.: Modelling the impacts of reservoir operations on the downstream riparian vegetation and fish habitats in the Lijiang River, J. Hydroinformatics, 13(2), 229, doi:10.2166/hydro.2010.008, 2011.

Liang, X., Lettenmaier, D. P., Wood, E. F. and Burges, S. J.: A simple hydrologically based model of land surface water and energy fluxes for general circulation model, J. Geophys. Res., 99(D7), 14,415–14,428, 1994.

Lobligeois, F., Andréassian, V., Perrin, C., Tabary, P. and Loumagne, C.: When does higher spatial resolution rainfall information improve streamflow simulation? An evaluation using 3620 flood events, Hydrol. Earth Syst. Sci., 18(2), 575–594, doi:10.5194/hess-18-575-2014, 2014.

Longo, M.: Amazon Forest Response to Changes in Rainfall Regime: Results from an Individual-Based Dynamic Vegetation Model, Harvard University. [online] Available from: http://dash.harvard.edu/handle/1/11744438, 2014.

Medvigy, D., Wofsy, S. C., Munger, J. W., Hollinger, D. Y. and Moorcroft, P. R.: Mechanistic scaling of ecosystem function and dynamics in space and time: Ecosystem Demography model version 2, J. Geophys. Res. Biogeosciences, 114(G1), G01002, doi:10.1029/2008JG000812, 2009.

Medvigy, D., Walko, R. L. and Avissar, R.: Effects of Deforestation on Spatiotemporal Distributions of Precipitation in South America, J. Clim., 24(8), 2147–2163, doi:10.1175/2010JCLI3882.1, 2011.

Miller, W. A. and Cunge, J. A.: Simplified equations of unsteady flow, in Unsteady Flow in Open Channels, edited by K. Mahmood and V. Yevjevich., 1975.

Mohor, G. S., Rodriguez, D. A., Tomasella, J. and Siqueira Júnior, J. L.: Exploratory analyses for the assessment of climate change impacts on the energy production in an Amazon run-of-river hydropower plant, J. Hydrol. Reg. Stud., 4, 41–59, doi:10.1016/j.ejrh.2015.04.003, 2015.

Moorcroft, P. R., Hurtt, G. C. and Pacala, S. W.: A method for scaling vegetation dynamics: The ecosystem demography model (ED), Ecol. Monogr., 71(4), 557–586, doi:10.1890/0012-9615(2001)071[0557:AMFSVD]2.0.CO;2, 2001.

Nash, E. and Sutcliffe, V.: River flow forecasting Through conceptual models PART I- A Discussion of principles, J. Hydrol., 10, 282–290, 1970.

Oki, T., Nishimura, T. and Dirmeyer, P.: Assessment of Annual Runoff from Land Surface Models Using Total Runoff Integrating Pathways (TRIP), J. Meteorol. Soc. Japan, 77(1B), 235–255 [online] Available from: https://www.jstage.jst.go.jp/article/jmsj1965/77/1B/77_1B_235/_article, 1999.

Oki, T., Agata, Y., Kanae, S., Saruhashi, T., Yang, D. and Musiake, K.: Global assessment of current water resources using total runoff integrating pathways, Hydrol. Sci. J., 46(6), 983–995, doi:10.1080/02626660109492890, 2001.

Oleson, K. W., Lawrence, D. M., Bonan, G. B., Flanner, M. G., Kluzek, E., Lawrence, P. J., Levis, S., Swenson, S. C. and Thornton, P. E.: Technical Description of version 4.0 of the

Community Land Model (CLM), Boulder, CO - USA. [online] Available from: http://www.cesm.ucar.edu/models/cesm1.0/clm/CLM4_Tech_Note.pdf, 2010.

Ostberg, S., Schaphoff, S., Lucht, W. and Gerten, D.: Three centuries of dual pressure from land use and climate change on the biosphere, Environ. Res. Lett., 10(4), 044011, doi:10.1088/1748-9326/10/4/044011, 2015.

Paiva, R. C. D., Collischonn, W. and Tucci, C. E. M.: Large scale hydrologic and hydrodynamic modeling using limited data and a GIS based approach, J. Hydrol., 406(3-4), 170–181, doi:10.1016/j.jhydrol.2011.06.007, 2011.

Paiva, R. C. D., Buarque, D. C., Collischonn, W., Bonnet, M. P., Frappart, F., Calmant, S. and Bulhões Mendes, C. A.: Large-scale hydrologic and hydrodynamic modeling of the Amazon River basin, Water Resour. Res., 49(3), 1226–1243, doi:10.1002/wrcr.20067, 2013a.

Paiva, R. C. D., Collischonn, W. and Buarque, D. C.: Validation of a full hydrodynamic model for large-scale hydrologic modelling in the Amazon, Hydrol. Process., 27(3), 333–346, doi:10.1002/hyp.8425, 2013b.

Paz, A. R., Collischonn, W. and Lopes da Silveira, A. L.: Improvements in large-scale drainage networks derived from digital elevation models, Water Resour. Res., 42(8), doi:10.1029/2005WR004544, 2006.

Pearson, K.: Note on regression and inheritance in the case of two parents, Proc. R. Soc. London, 58, 1895.

Pearson, R. G., Phillips, S. J., Loranty, M. M., Beck, P. S. A., Damoulas, T., Knight, S. J. and Goetz, S. J.: Shifts in Arctic vegetation and associated feedbacks under climate change, Nat. Clim. Chang., 3(7), 673–677, doi:10.1038/nclimate1858, 2013.

Pontes, P. R. M., Collischonn, W., Fan, F. M., Paiva, R. C. D. and Buarque, D. C.: Modelagem hidrológica e hidráulica de grande escala com propagação inercial de vazões, Rev. Bras. Recur. Hídricos, 20(4), 888–904, 2015.

Poorter, L., Bongers, L. and Bongers, F.: Architecture of 54 moist-forest tree species: traits, trade-offs, and functional groups, Ecology, 87(5), 1289–1301, doi:10.1890/0012-9658(2006)87[1289:AOMTST]2.0.CO;2, 2006.

Prigent, C., Papa, F., Aires, F., Rossow, W. B. and Matthews, E.: Global inundation dynamics inferred from multiple satellite observations, 1993–2000, J. Geophys. Res., 112(D12), D12107, doi:10.1029/2006JD007847, 2007.

Quesada, C. A., Lloyd, J., Schwarz, M., Patiño, S., Baker, T. R., Czimczik, C., Fyllas, N. M., Martinelli, L., Nardoto, G. B., Schmerler, J., Santos, A. J. B., Hodnett, M. G., Herrera, R., Luizão, F. J., Arneth, A., Lloyd, G., Dezzeo, N., Hilke, I., Kuhlmann, I., Raessler, M., Brand, W. A., Geilmann, H., Moraes Filho, J. O., Carvalho, F. P., Araujo Filho, R. N., Chaves, J. E., Cruz Junior, O. F., Pimentel, T. P. and Paiva, R.: Variations in chemical and physical properties of Amazon forest soils in relation to their genesis, Biogeosciences, 7(5), 1515–1541, doi:10.5194/bg-7-1515-2010, 2010.

Raddatz, T. J., Reick, C. H., Knorr, W., Kattge, J., Roeckner, E., Schnur, R., Schnitzler, K.-G., Wetzel, P. and Jungclaus, J.: Will the tropical land biosphere dominate the climate–carbon cycle feedback during the twenty-first century?, Clim. Dyn., 29(6), 565–574, doi:10.1007/s00382-007-0247-8, 2007.

Reed, S. M.: Deriving flow directions for coarse-resolution (1-4 km) gridded hydrologic modeling, Water Resour. Res., 39(9), doi:10.1029/2003WR001989, 2003.

Rost, S., Gerten, D., Bondeau, A., Lucht, W., Rohwer, J. and Schaphoff, S.: Agricultural green and blue water consumption and its influence on the global water system, Water Resour. Res., 44(9), n/a–n/a, doi:10.1029/2007WR006331, 2008.

Sheffield, J., Goteti, G. and Wood, E. F.: Development of a 50-Year High-Resolution Global Dataset of Meteorological Forcings for Land Surface Modeling, J. Clim., 19(13), 3088–3111, doi:10.1175/JCLI3790.1, 2006.

Sitch, S., Smith, B., Prentice, I. C., Arneth, A., Bondeau, A., Cramer, W., Kaplan, J. O., Levis, S., Lucht, W., Sykes, M. T., Thonicke, K. and Venevsky, S.: Evaluation of ecosystem dynamics, plant geography and terrestrial carbon cycling in the LPJ dynamic global vegetation model, Glob. Chang. Biol., 9(2), 161–185, doi:10.1046/j.1365-2486.2003.00569.x, 2003.

Smith, M. B., Koren, V. I., Zhang, Z., Reed, S. M., Pan, J.-J. and Moreda, F.: Runoff response to spatial variability in precipitation: an analysis of observed data, J. Hydrol., 298(1-4), 267–286, doi:10.1016/j.jhydrol.2004.03.039, 2004.

Soares-Filho, B. S., Nepstad, D. C., Curran, L. M., Cerqueira, G. C., Garcia, R. A., Ramos, C. A., Voll, E., McDonald, A., Lefebvre, P. and Schlesinger, P.: Modelling conservation in the Amazon basin., Nature, 440(7083), 520–3, doi:10.1038/nature04389, 2006.

Swann, A. L. S., Longo, M., Knox, R. G., Lee, E. and Moorcroft, P. R.: Future deforestation in the Amazon and consequences for South American climate, Agric. For. Meteorol., 214-215, 12–24, doi:10.1016/j.agrformet.2015.07.006, 2015.

USACE: A Muskingum-Cunge Channel Flow Routing Method for Drainage Networks. [online] Available from: http://www.hec.usace.army.mil/publications/TechnicalPapers/TP-135.pdf, 1991.

Vamborg, F. S. E., Brovkin, V. and Claussen, M.: The effect of a dynamic background albedo scheme on Sahel/Sahara precipitation during the mid-Holocene, Clim. Past, 7(1), 117–131, doi:10.5194/cp-7-117-2011, 2011.

Walko, R. L., Band, L. E., Baron, J., Kittel, T. G. F., Lammers, R., Lee, T. J., Ojima, D., Pielke, R. A., Taylor, C., Tague, C., Tremback, C. J. and Vidale, P. L.: Coupled Atmosphere–Biophysics–Hydrology Models for Environmental Modeling, J. Appl. Meteorol., 39(6), 931–944, doi:10.1175/1520-0450(2000)039<0931:CABHMF>2.0.CO;2, 2000.

Wohl, E., Barros, A., Brunsell, N., Chappell, N. A., Coe, M., Giambelluca, T., Goldsmith, S., Harmon, R., Hendrickx, J. M. H., Juvik, J., McDonnell, J. and Ogden, F.: The hydrology of the humid tropics, Nat. Clim. Chang., 2(9), 655–662, doi:10.1038/nclimate1556, 2012.

Yamazaki, D., Kanae, S., Kim, H. and Oki, T.: A physically based description of floodplain inundation dynamics in a global river routing model, Water Resour. Res., 47(4), n/a–n/a, doi:10.1029/2010WR009726, 2011.

Zambrano-Bigiarini, M.: hydroGOF: Goodness-of-fit functions for comparison of simulated and observed hydrological time series. R package version 0.3-8, [online] Available from: http://cran.r-project.org/package=hydroGOF, 2014.

Zhang, K., de Almeida Castanho, A. D., Galbraith, D. R., Moghim, S., Levine, N. M., Bras, R. L., Coe, M. T., Costa, M. H., Malhi, Y., Longo, M., Knox, R. G., McKnight, S., Wang, J. and Moorcroft, P. R.: The fate of Amazonian ecosystems over the coming century arising from changes in climate, atmospheric CO2, and land use, Glob. Chang. Biol., 21(7), 2569–2587, doi:10.1111/gcb.12903, 2015.

Zulkafli, Z., Buytaert, W., Onof, C., Lavado, W. and Guyot, J. L.: A critical assessment of the JULES land surface model hydrology for humid tropical environments, Hydrol. Earth Syst. Sci., 17(3), 1113–1132, doi:10.5194/hess-17-1113-2013, 2013.

Figures

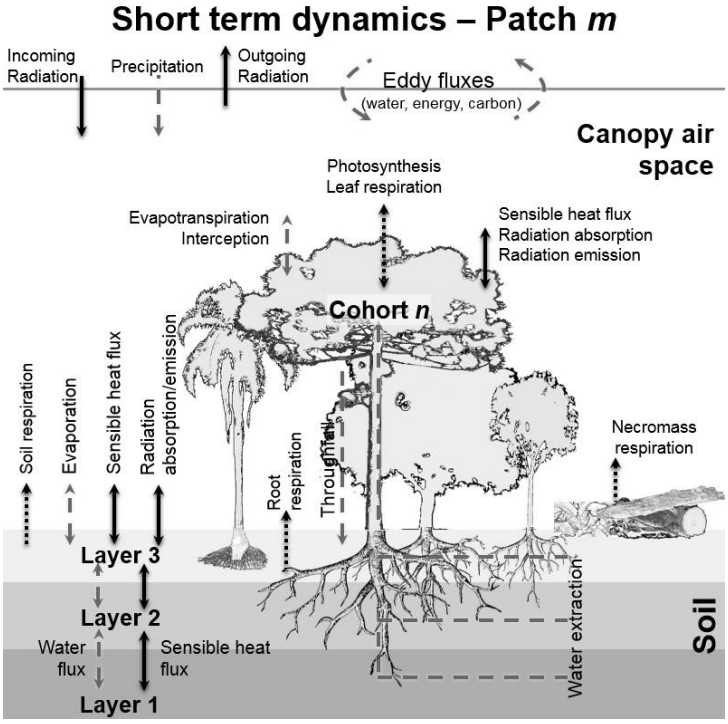

Figure 1. Schematic of the enthalpy fluxes (all arrows) and water fluxes (all but solid black arrows) that are solved in ED2. The schematic is based on Walko et al. (2000); and Medvigy et al. (2009). (Courtesy of Marcos Longo).

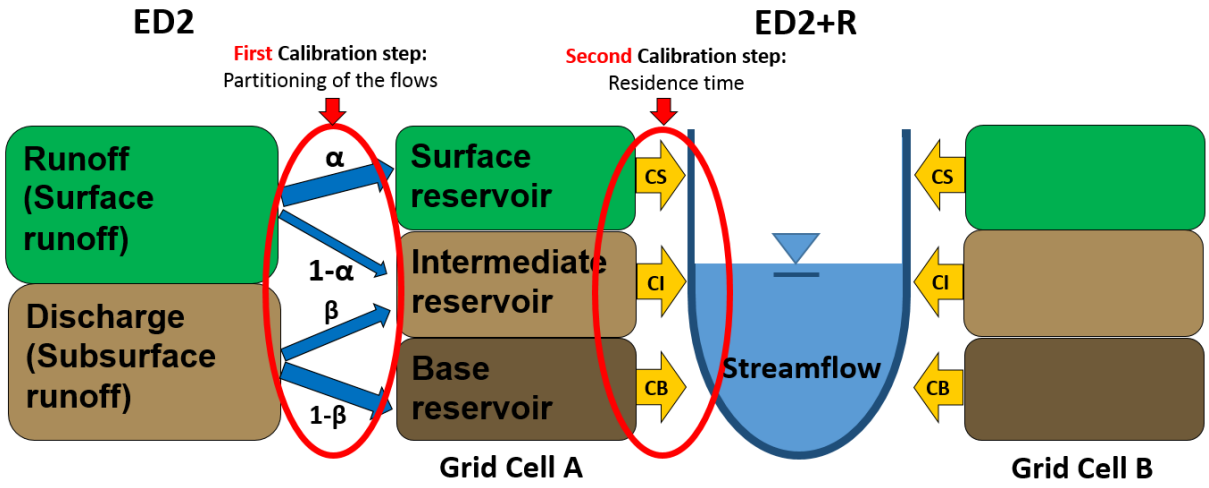

Figure 2. Schematic representation of the connection between the terrestrial biosphere model and the hydrological routing scheme. Calibrating parameters circled in red. The reservoirs are used to determine the contribution of streamflow that comes from overland flow, interflow and groundwater flow. The daily sum of these three reservoirs is then moved from each grid cell into the drainage network.

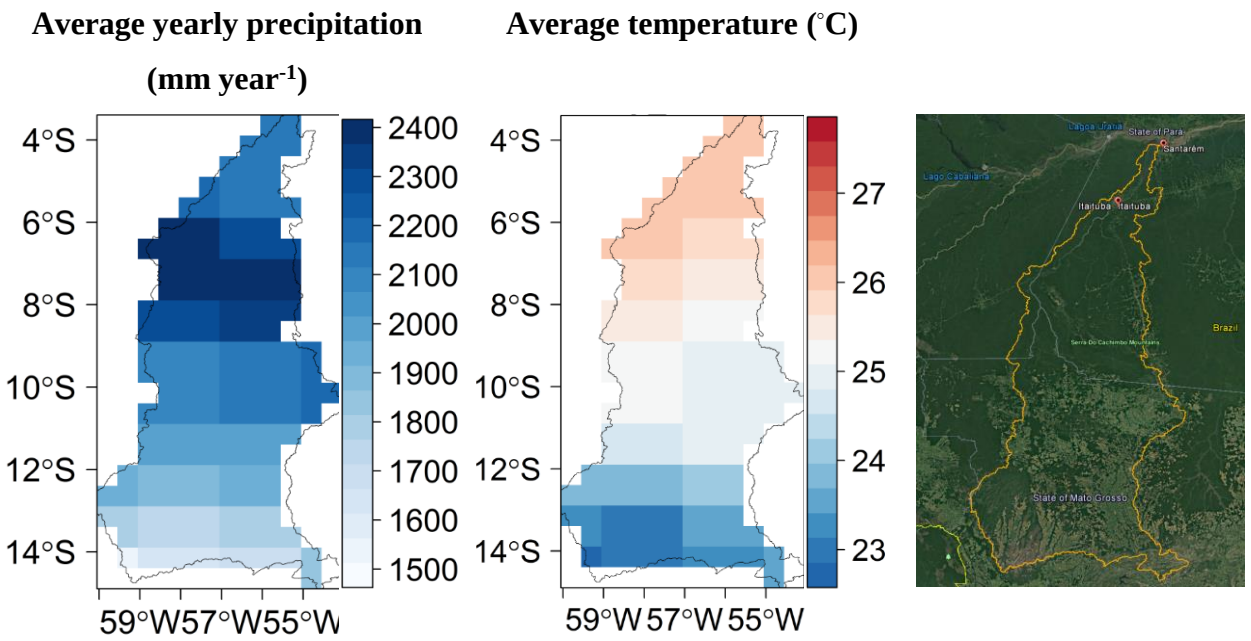

(a) (b) (c)

1 Figure 3. Average precipitation (a) and temperature (b) in the Tapajós river basin (1986 - 2005).
2 Redrafted from Farinosi et al. (under review). (c) Land use in the Tapajós river basin. Source:
3 Google Earth Pro.

4

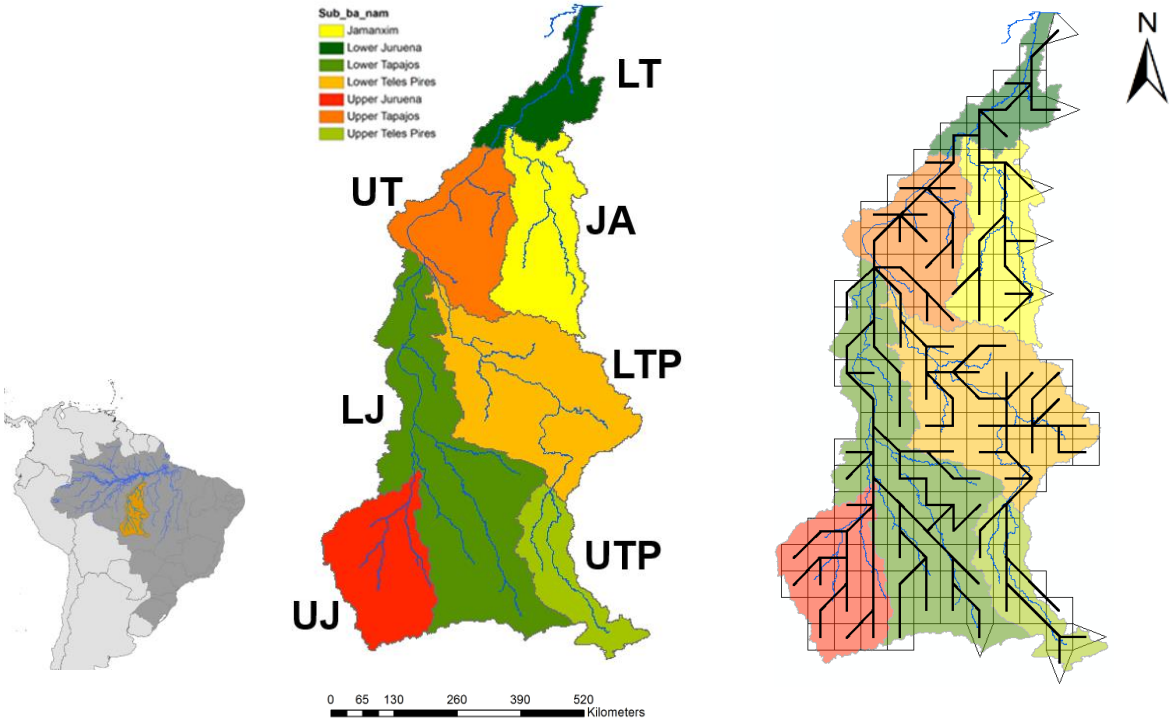

(a) (b)

Figure 4. (a) Organization of the Tapajós basin into seven sub-basins: Upper Juruena (UJ); Lower Juruena (LJ); Upper Teles Pires (UTP); Lower Teles Pires (LTP); Jamanxim (JA); Upper Tapajós (UT); and Lower Tapajós (LT). (b) ED2+R represents the domain in grid cells with 0.5° resolution (~ 55 km). The black segments indicate flow accumulation network.

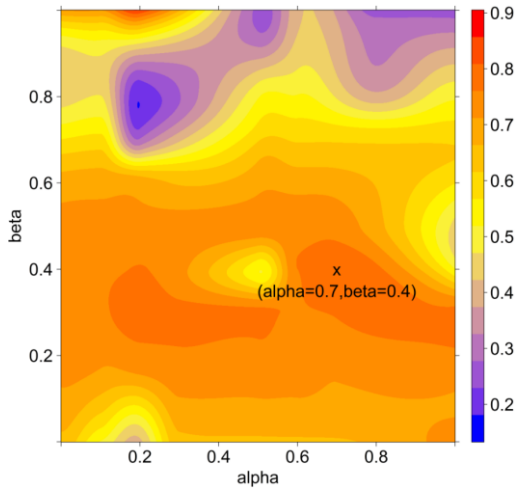

Figure 5. Calibration of flow partitioning (parameters alpha and beta in Figure 2) between the ED2 and the ED2+R reservoirs. Color bar indicates the NSE values of the simulated versus the observed river flow values (0 very different, 1 very similar)

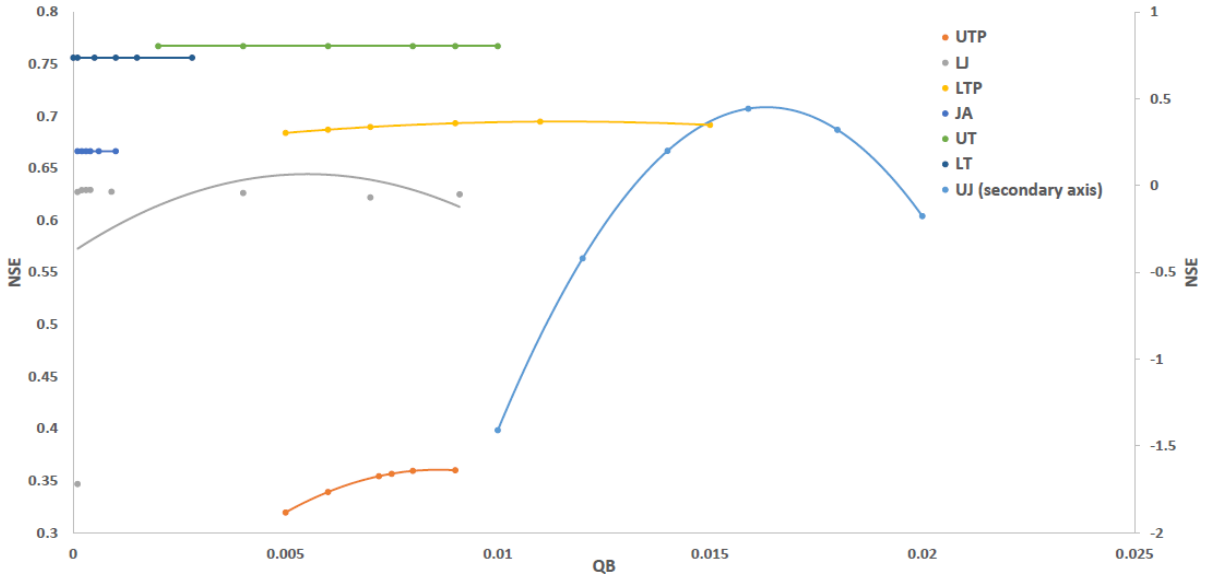

Figure 6. Initial conditions of baseflow sensitivity for different ED2+R subbasins in the domain. Upper Juruena (UJ); Upper Teles Pires (UTP); Lower Juruena (LJ); Lower Teles Pires (LTP); Upper Tapajós (UT); Jamanxim (JA); and Lower Tapajós (LT).

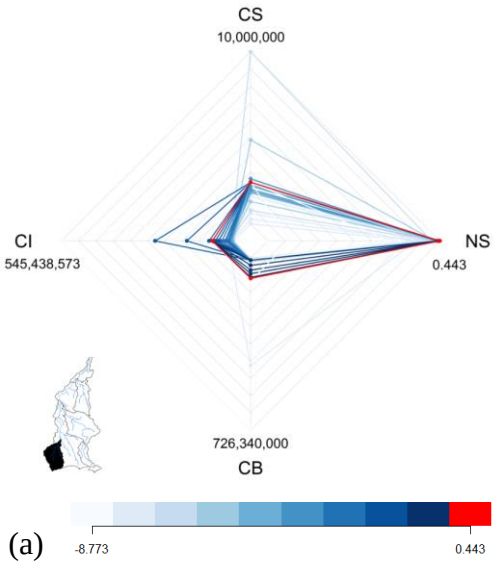
CS
10,000,000
CI
545,438,573
NS
0.443
726,340,000
CB
-8.773
0.443

(a)

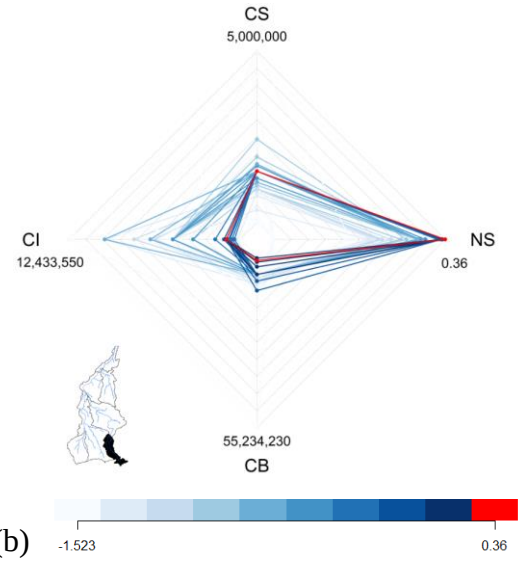
CS
5,000,000
CI
12,433,550
NS
0.36
55,234,230
CB
-1.523
0.36

(b)

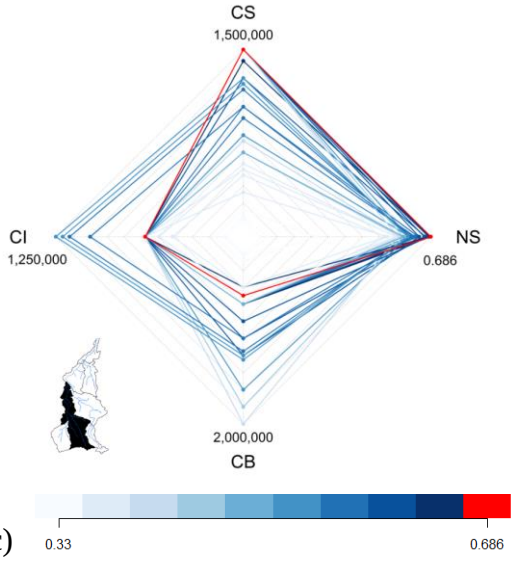
CS
1,500,000
CI
1,250,000
NS
0.686
2,000,000
CB
0.33
0.686

(c)

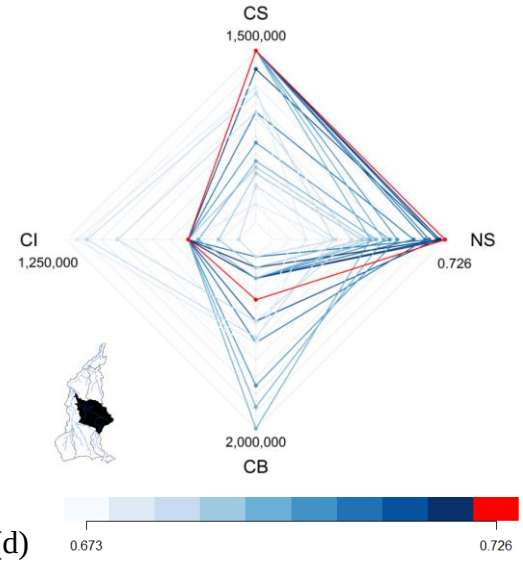
CS
1,500,000
CI
1,250,000
NS
0.726
2,000,000
CB
0.673
0.726

(d)

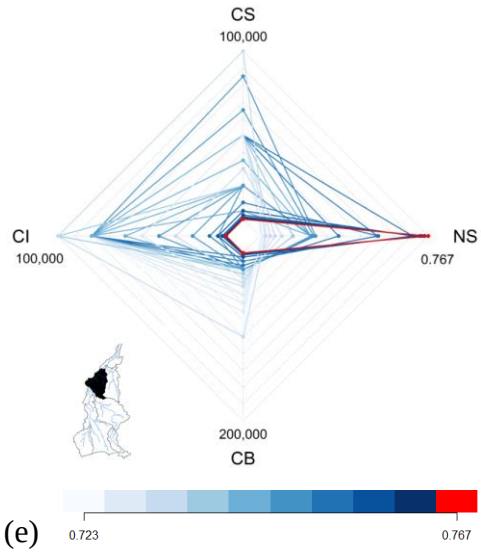
CS
100,000
CI
100,000
NS
0.767
200,000
CB
0.723
0.767

(e)

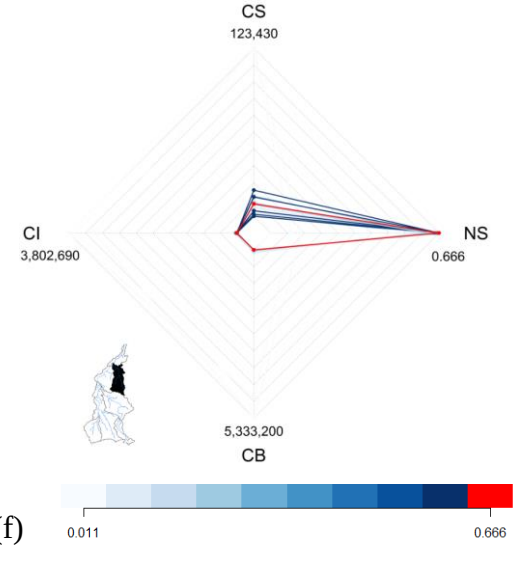
CS
123,430
CI
3,802,690
NS
0.666
5,333,200
CB
0.011
0.666

(f)

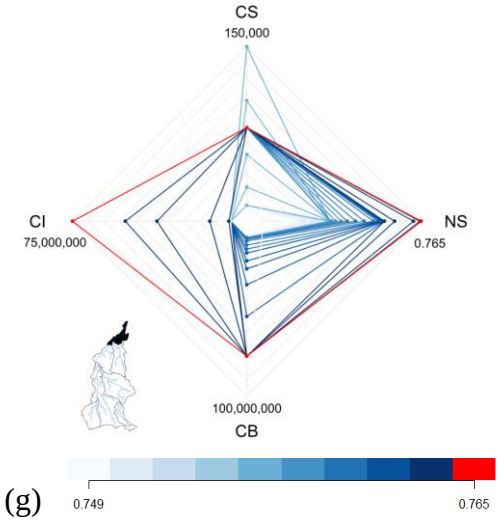

(g)

Figure 7. Calibration of the residence times (τ) of the flow within the ED2+R reservoirs of different grid cells in the domain. Overland, intermediate and groundwater flows are indicated respectively by CS, CI, and CB (Figure 2). In red the chosen combination. (a) Upper Juruena (UJ); (b) Upper Teles Pires (UTP); (c) Lower Juruena (LJ); (d) Lower Teles Pires (LTP); (e) Upper Tapajós (UT); (f) Jamanxim (JA); and (g) Lower Tapajós (LT).

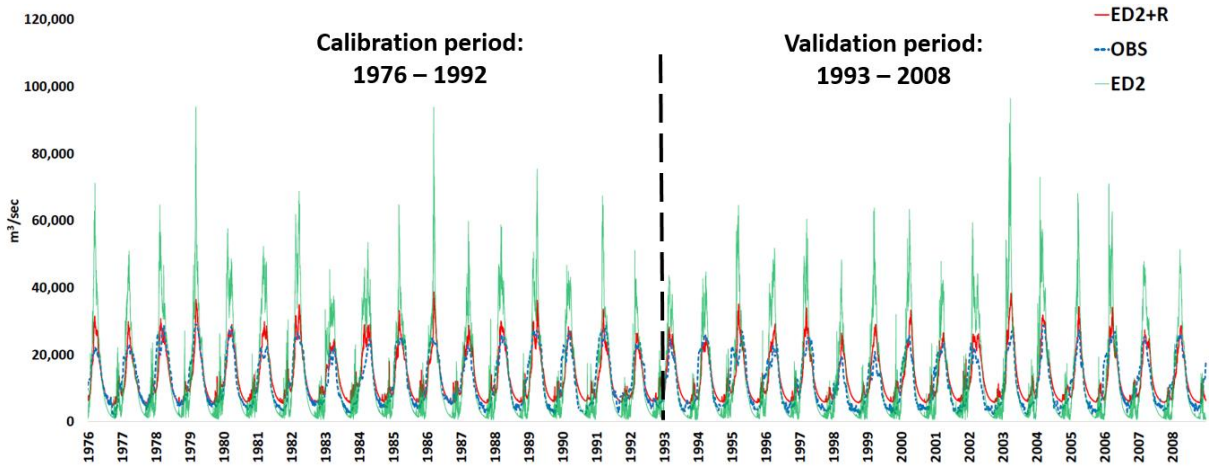

Figure 8. Calibration and validation of the river flow (m^3/sec) at Itaituba (farthest downstream river gauge – Lower Tapajós sub-basin). ED2 output (green line), ED2+R (red line), and Observations (blue dotted line). The dotted black line splits the calibration and validation periods. Similar comparison for each of the 7 sub-basins is available in Annex A.

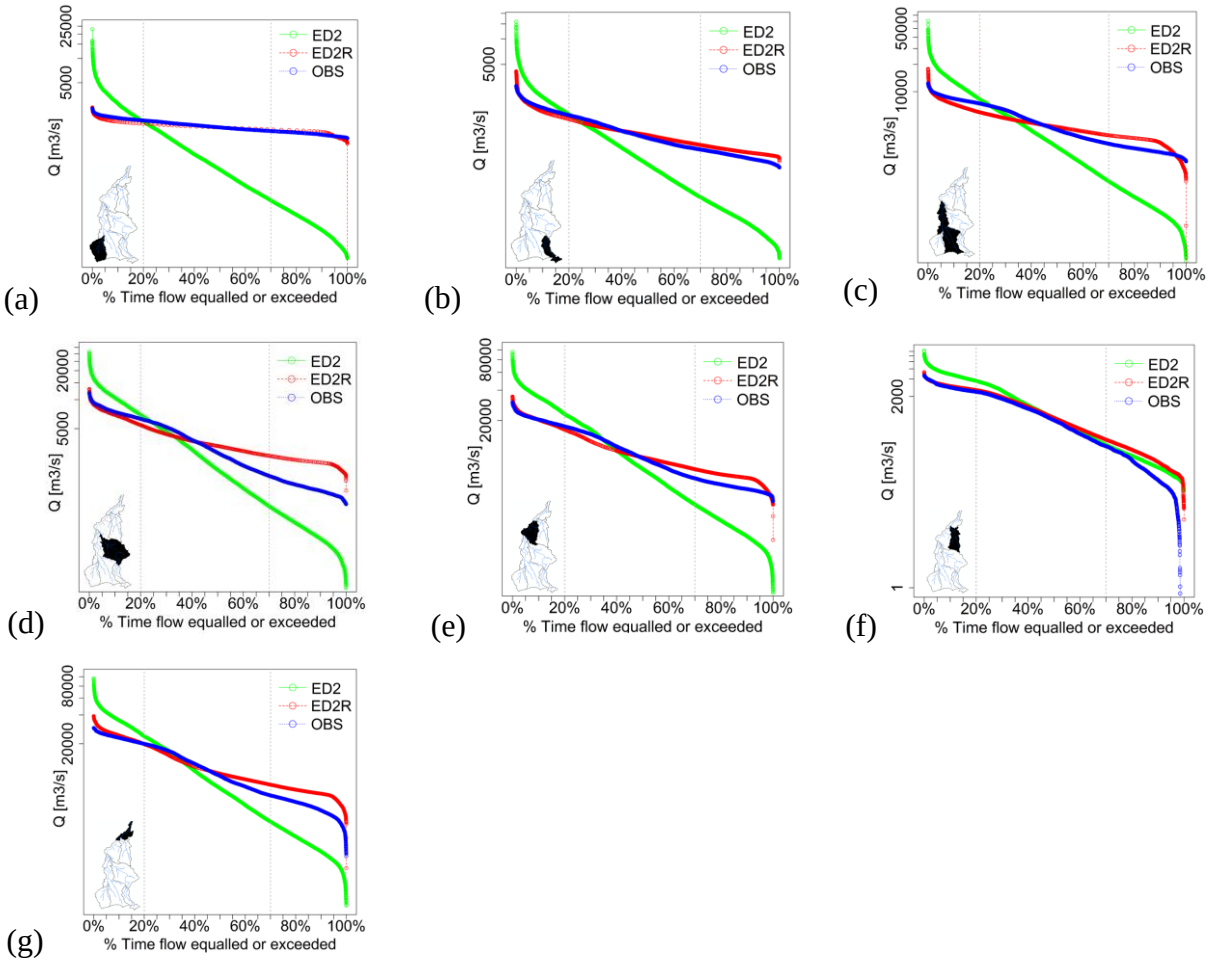

Figure 9. Flow duration curves (percentage of time that flow – m^3/s – is likely to equal or exceed determined thresholds) of observed values (blue), ED2 outputs (green), ED2+R (red) at the outlet of the seven sub-basins. (a) Upper Juruena (UJ); (b) Upper Teles Pires (UTP); (c) Lower Juruena (LJ); (d) Lower Teles Pires (LTP); (e) Upper Tapajós (UT); (f) Jamanxim (JA); and (g) Lower Tapajós (LT).

Tables

Table 1. ED2+R parameters (based on Zhang et al., 2015; Longo et al., 2014; Knox et al., 2012)

Input	**Source**	
Meteorological forcing	Sheffield et al. (2006)	
Land use	Hurtts et al. (2006)	
Topography (DEM)	SRTM, Shuttle Radar Topography Mission 90 mt resolution	
Soil data	Quesada et al. (2010) -IGBP-DIS global soil data (Global Soil Data Task 2014)	
Geomorphological relations	Coe et al. (2008)	
Streamflow observations	HYBAM - ANA	
Carbon dioxide concentration	378 ppm	
Process	**Method**	
Integration scheme	4th order Runge-Kutta method	
Energy and water cycles	Knox (2012) and Longo (2014)	
Temperature-dependent function for photosynthesis	Q_{10} function	
Canopy radiation scheme	Two-stream model	
Allometry for height	Based on Poorter et al. (2006)	
Allometry for above-ground biomass	Based on Eqn. (2) of Baker et al. (2004)	
Allometry for leaf biomass	Based on Cole & Ewel (2006) and Calvo-Alvarado et al. (2008)	
Parameter	**Value**	**Units**
Biophysics time step	600	s
Number of soil layers	16	-
Depth of the deepest soil layer	6	m
Depth of the shallowest soil layer	0.02	m
Cohort water holding capacity	0.11	$kg_w m_{leaf+wood}^{-2}$
Residual stomatal conductance	10,000	$\mu mol\ m^{-2} s^{-1}$
Leaf-level water stress parameter	0.016	$mol_{H_2O}\ mol_{Air}^{-1}$
Oxygenase/carboxylase ratio at 15ºC	4000	-
Power base for oxygenase/carboxylase ratio	0.57	-
Power base for carboxylation rate	2.4	-
Power base for dark respiration rate	2.4	-
Environmentally-determined parameters	**Value**	**Units**
Weight factor for stress due to light	1.0	-
Maximum environmentally-determined mortality rate	5.0	yr^{-1}
Steepness of logistic curve	10.0	-
Band-dependent radiation parameters (*)	**Value**	**Units**
Dry soil reflectance	(0.20; 0.31; 0.02)	-
Wet soil reflectance	(0.10; 0.20; 0.02)	-
Leaf transmittance	(0.05; 0.20; 0.00)	-
Leaf reflectance (grasses)	(0.10; 0.40; 0.04)	-
Leaf reflectance (trees)	(0.10; 0.40; 0.05)	-
Wood transmittance	(0.05; 0.20; 0.00)	-
Wood reflectance (trees)	(0.05; 0.20; 0.10)	-
Plant Functional Type PFT-dependent parameters (**)	**Value**	**Units**
Leaf orientation factor	(0.10; 0.10; 0.10)	-
Leaf clumping factor	(0.80; 0.80; 0.80)	-

Leaf characteristic size	(0.10; 0.10; 0.10)	m
Max. carboxylation rate at 15ºC	(18.75; 12.50; 6.25)	$\mu mol_C\ m_{leaf}^{-2} s^{-1}$
Dark respiration rate at 15ºC	(0.272; 0.181; 0.091)	$\mu mol_C\ m_{leaf}^{-2} s^{-1}$
Quantum yield	(0.080; 0.080; 0.080)	-
Slope parameter for stomatal conductance	(9.0; 9.0; 9.0)	-
Fine root conductance parameter	(600; 600; 600)	$m^2 kg_{C_{root}}^{-1} yr^{-1}$
River Routing Parameters (Section 4)	**Value**	**Units**
Grid-cell size (Figure 4)	0.5x0.5	*degrees*
Flow partitioning parameters (α; β) (Figure 5)	(0.70; 0.40)	-
Residence time Overland (CS), intermediate (CI), and groundwater flows (CB) (Figure 7) (CS; CI; CB)	Upper Juruena (2,600; 70,000; 90,000) Upper Teles Pires (1,600; 1,750; 2,500) Lower Juruena (1,500; 600; 500) Lower Teles Pires (1,500; 650; 800) Jamanxim (10; 10; 11) Upper Tapajós (75; 75,000; 75,000) Lower Tapajós (75; 75,000; 75,000)	*x1 '000 (***)*
Initial conditions of the baseflow (Figure 6)	Upper Juruena (0.0159) Upper Teles Pires (0.009) Lower Juruena (0.0004) Lower Teles Pires (0.011) Jamanxim (0.0001) Upper Tapajós (0.0080) Lower Tapajós (0.0005)	$m^3 km^2$

(*) Radiation-dependent parameters are given in the format (xPAR; xNIR; xTIR) corresponding to values for photosynthetically active, near infrared and thermal infrared, respectively.
(**) PFT-dependent parameters are given in the format (xETR; xMTR; xLTR) corresponding to the values for early-, mid-, and late-successional cohorts, respectively.
(***)The residence time parameters are dimensionless and used to correct the Kirpich formula for time of concentration as explained in Collischonn et al. (2007). Their magnitude is influenced by the size of the grid-cell.

1

2

Table 2. Statistics about the gauge information filling procedure (correlation with the station to be filled, number of original observations, filled number of observations).

Sub-basin name	Main river gauge station - **z** in Equation 7	Original number of daily gauge records (number of daily observations)	Gap filling station 1 – **q** in Equation 7 – [correlation with **z]**	Gap filling station 2 – **y** in Equation 7 – [correlationwith **z]**	Number of daily records after filling procedure (number of daily observations)
Jamanxin	Jamanxim	1,928	Jardim do Ouro [0.97]	Novo Progresso [0.96]	5,382
Upper Teles Pires	Cachoeirão	10,356	Teles Pires [0.91]	Indeco [0.94]	11,524
Upper Juruena	Fontanilhas	10,469	Foz do Juruena [0.94]	Barra do Sao Manuel [0.89]	11,688
Lower Teles Pires	Tres Marias	8,682	Barra do Sao Manuel [0.98]	Santa Rosa [0.98]	10,640
Lower Juruena	Foz do Juruena	2,074	Barra do Sao Manuel [0.98]	Jatoba [0.97]	11,447
Upper Tapajós	Jatoba	10,218	Fortaleza [0.99]	Barra do Sao Manuel [0.98]	11,517
Lower Tapajós	Itaituba	5,789	Fortaleza [0.99]	Jatoba [0.98]	11,688

Table 3. Calibration and validation results. Nash-Sutcliffe Efficiency, Kling Gupta (2009 and 2012 methods), Pearson's R correlation, and volume ratio. Optimal values = 1 (statistics where calculated using the R package hydroGOF - Zambrano-Bigiarini 2014).

Sub-basin	Calibration period (1976-1992)								Validation period (1993-2008)							
	Nash-Sutcliffe		Kling-Gupta [method 2009] {method 2012}		Pearson's R Correlation		Volume Ratio Vol sim/Vol Obs		Nash-Sutcliffe		Kling-Gupta [method 2009] {method 2012}		Pearson's R Correlation		Volume Ratio Vol sim/Vol Obs	
	ED vs OBS	ED2+R vs OBS	ED vs OBS	ED2+R vs OBS	ED vs OBS	ED2+R vs OBS	ED vs OBS	ED2+R vs OBS	ED vs OBS	ED2+R vs OBS	ED vs OBS	ED2+R vs OBS	ED vs OBS	ED2+R vs OBS	ED vs OBS	ED2+R vs OBS
Upper Juruena	-26.88	0.45	[-3.60] {-5.75}	[0.50] {0.51}	0.61	0.68	0.72	0.98	-27.47	0.29	[-3.54] {-6.10}	[0.39] {0.38}	0.53	0.54	0.68	1.01
Upper Teles Pires	-3.35	0.37	[-0.51] {-0.64}	[0.61] {0.61}	0.53	0.64	0.94	1.01	-3.19	0.28	[-0.51] {-0.59}	[0.63] {0.63}	0.57	0.63	0.96	1.03
Lower Juruena	-1.45	0.65	[-0.23] {-0.18}	[0.64] {0.67}	0.77	0.82	1.02	0.94	-2.17	0.63	[-0.43] {-0.30}	[0.72] {0.67}	0.75	0.81	1.05	1.08
Lower Teles Pires	-0.20	0.71	[0.25] {0.27}	[0.68] {0.67}	0.80	0.85	1.01	1.02	-0.34	0.67	[0.17] {0.34}	[0.69] {0.60}	0.82	0.85	1.11	1.17
Jamanxim	-0.74	0.67	[0.01] {0.39}	[0.79] {0.78}	0.82	0.85	1.55	1.13	-0.10	0.55	[0.23] {0.52}	[0.75] {0.73}	0.83	0.77	1.43	1.09
Upper Tapajós	-1.01	0.77	[-0.13] {0.21}	[0.82] {0.83}	0.84	0.88	1.20	0.99	-1.23	0.75	[-0.22] {0.16}	[0.84] {0.81}	0.84	0.88	1.21	1.08
Lower Tapajós	-0.40	0.76	[-0.09] {0.28}	[0.86] {0.83}	0.84	0.88	1.11	1.06	-0.50	0.68	[0.09] {0.29}	[0.80] {0.76}	0.82	0.86	1.13	1.13

1 **Annex A**

2

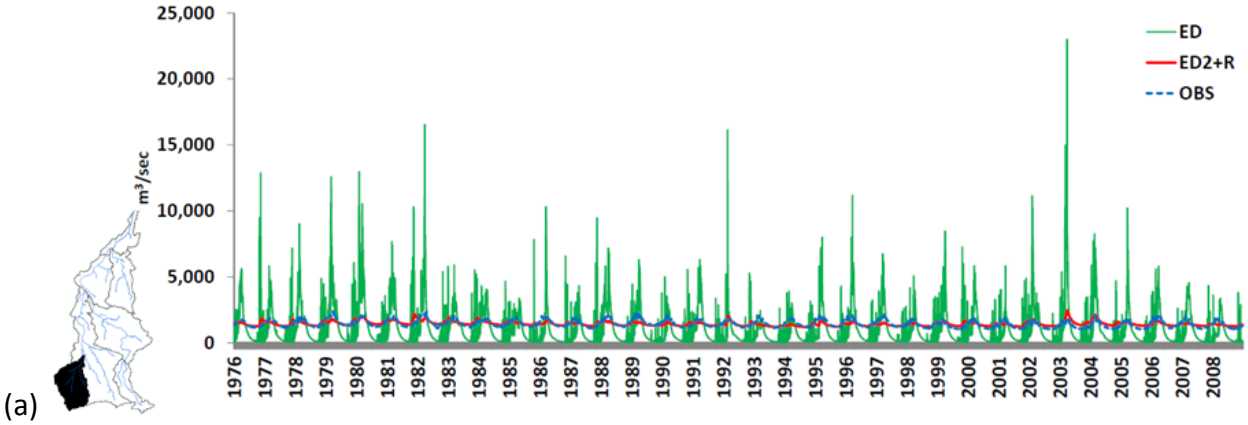

(a)

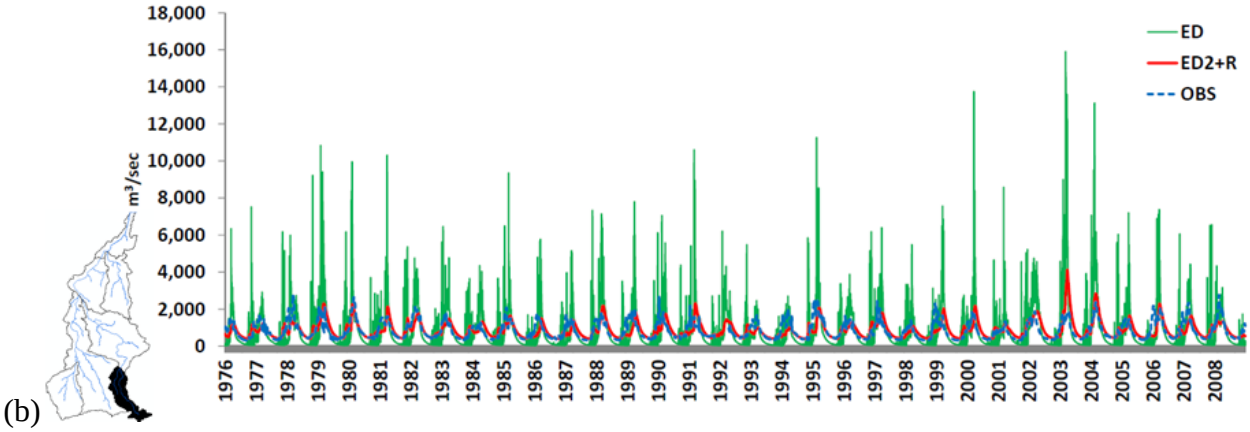

(b)

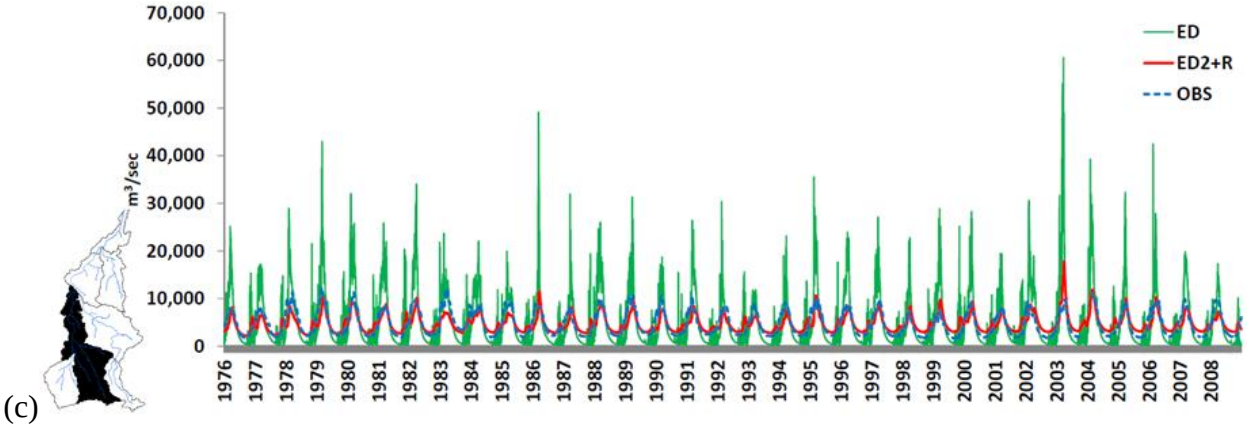

(c)

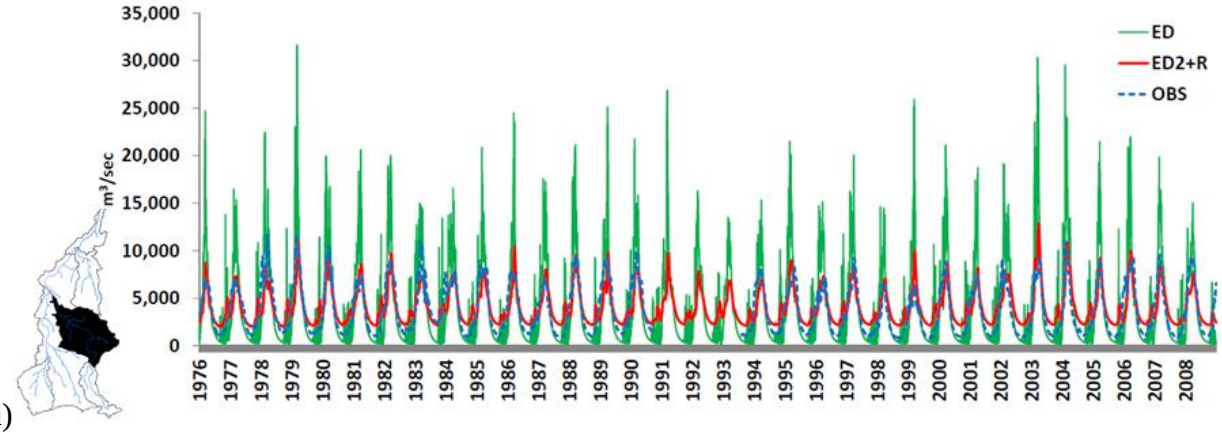
35,000
30,000
25,000
20,000
15,000
10,000
5,000
0
m³/sec
ED
ED2+R
OBS
1976 1977 1978 1979 1980 1981 1982 1983 1984 1985 1986 1987 1988 1989 1990 1991 1992 1993 1994 1995 1996 1997 1998 1999 2000 2001 2002 2003 2004 2005 2006 2007 2008

(d)

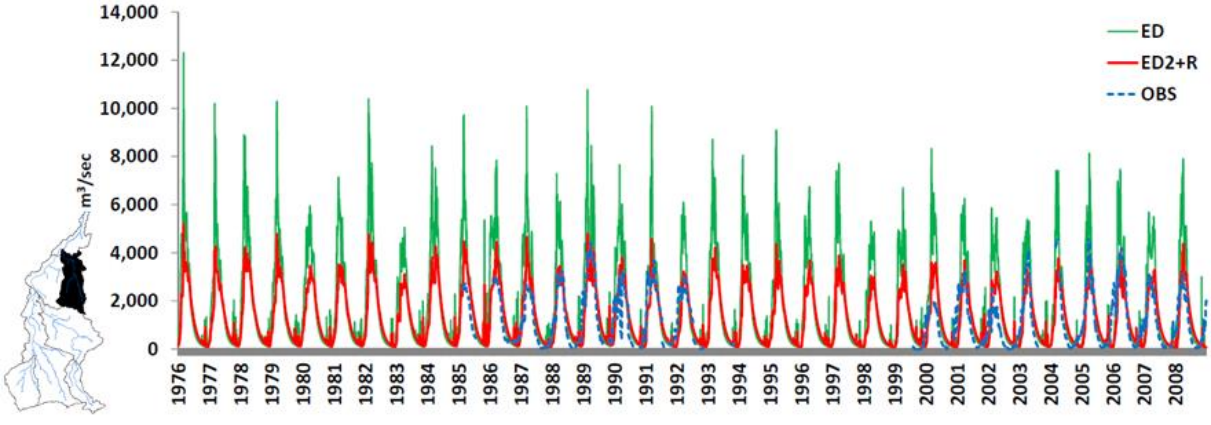
14,000
12,000
10,000
8,000
6,000
4,000
2,000
0
m³/sec
ED
ED2+R
OBS
1976 1977 1978 1979 1980 1981 1982 1983 1984 1985 1986 1987 1988 1989 1990 1991 1992 1993 1994 1995 1996 1997 1998 1999 2000 2001 2002 2003 2004 2005 2006 2007 2008

(e)

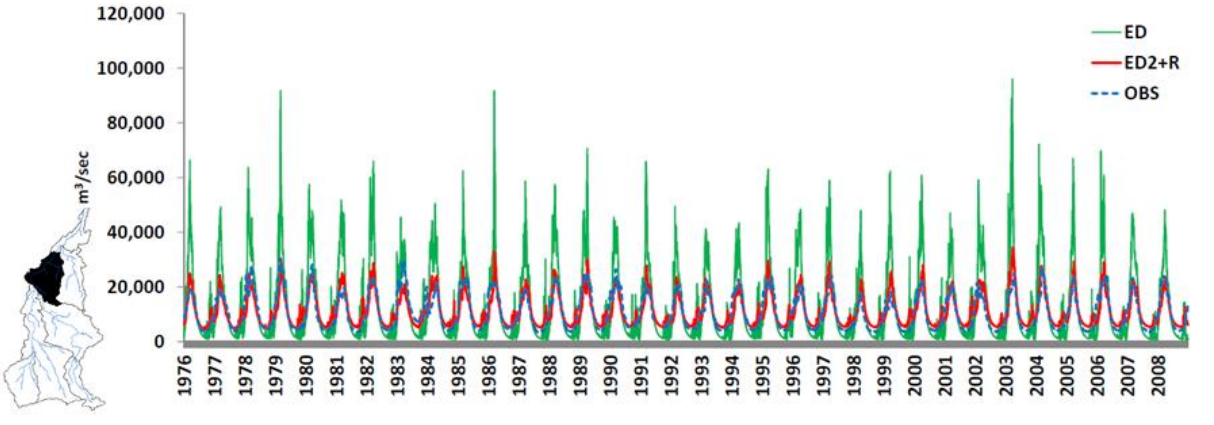
120,000
100,000
80,000
60,000
40,000
20,000
0
m³/sec
ED
ED2+R
OBS
1976 1977 1978 1979 1980 1981 1982 1983 1984 1985 1986 1987 1988 1989 1990 1991 1992 1993 1994 1995 1996 1997 1998 1999 2000 2001 2002 2003 2004 2005 2006 2007 2008

(f)

(g)

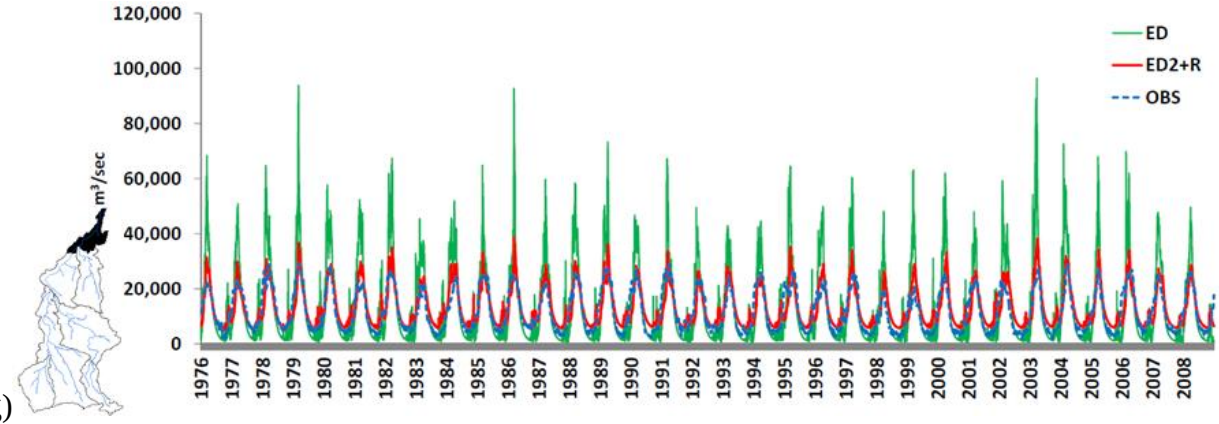

Figure A1. Time series of river flow (m3/sec) at the outlet of each sub-basins. ED2 output (green line), ED2+R (red line), and Observations (blue dotted line). (a) Upper Juruena (UJ); (b) Upper Teles Pires (UTP); (c) Lower Juruena (LJ); (d) Lower Teles Pires (LTP); (e) Jamanxim (JA); (f) Upper Tapajós (UT); and (g) Lower Tapajós (LT).